國 立 交 通 大 學

電信工程學系

碩 士 論 文

超寬頻多輸入多輸出系統模型之建構與量測

Modeling and Measurement of UWB MIMO Radio Channels

研究生： 蔡孟勳

指導教授：唐震寰博士

中 華 民 國 九十四 年 十 月

超寬頻多輸入多輸出系統模型之建構與測量
Modeling and Measurement of UWB MIMO Radio Channels

研 究 生：蔡孟勳　　Student : Mun-Xuin Tsai

指導教授：唐震寰　　Advisor : Dr. Jenn-Hwan Tarng

國 立 交 通 大 學

電 信 工 程 學 系 碩 士 班

碩 士 論 文

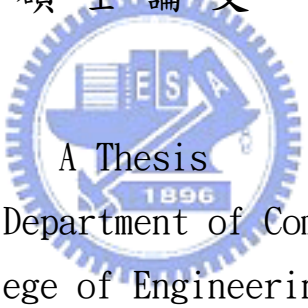

A Thesis

Submitted to Department of Communication

College of Engineering

National Chiao Tung University

in Partial Fulfillment of the Requirements

for the Degree of

Master of Science

in

Communication Engineering

October 2005

Hsinchu, Taiwan, Republic of China

中 華 民 國 九 十 四 年 十 月

超寬頻多輸入多輸出系統模型之建構與量測

研究生：蔡孟勳　　指導教授：唐震寰 博士

國立交通大學

電信工程學系碩士班

摘要

近幾年高傳輸速率特別受到重視，例如第三代行動通訊的標準如 WCDMA 和 UWB。基於需要較高的傳輸速率，我們結合 UWB 和 MIMO 的特性。本論文介紹在 UWB MIMO 系統中，傳播環境中的傳輸端與接收端的距離、本地散射體、相鄰的天線間距及天線的擺放方式對通道容量及相關性的影響。此外在本論文中也提出了適用於室內 UWB MIMO 的通道模型，此通道模型主要是先找出 UWB 的特性再根據 802.11n 通道模型去做結合的動作。

在本論文中，吾人發現了下列幾個現象：(1)在具有雜亂回波的環境下，在不同的接收距離下並不會對通道容量有任何影響;(2)在有本地散射體的環境下，通道容量會高於沒有本地散射體的環境; (3)通道容量會隨著天線單元間距的增加而增加，但在超過 0.5 波長後，天線單元間距對於通道容量就沒有顯著的影響;(4)在直接波存在的情況下，天線的擺放方式對通道容量是有影響的;(5)因為高相關性所造成的通道容量損失，會隨著 SNR 的增加而獲得補償;(6)在採用 S-V 模型的 UWB 系統中，可觀察到在直接波存在的情況下，參數Γ衰減的比沒有直接波存在的情況快;(7)我們發展的室內 UWB MIMO 通道模型，經由與量測結果的比較結果發現我們的通道模型是可適用於 UWB MIMO 系統。

Modeling and Measurement of UWB MIMO Radio Channels

Student：Mun-Xuin Tsai　　Advisor：Dr. Jenn-Hwan Tarng

Department of Communication Engineering

National Chiao Tung University

Abstract

Recent years have seen the emergence of high data rate, third generation wideband wireless communication standards like wideband code division multiple access (W-CDMA) and UWB radio. Motivated by the ever increasing demand for higher wideband wireless data rates, we consider multiple antenna communication over the UWB wireless channel (UWB-MIMO). In this thesis, we will introduce the capacity and correlation properties of UWB-MIMO channels and analyze the measured UWB-MIMO channel data to investigate the effects of propagation range, local scatterer, antenna spacing and array orientation effect. And in order to propose a set of channel models applicable to indoor UWB-MIMO systems. We first present the characterization of UWB channels for indoor environment with above measured data. Then we base on 802.11n channel model to develop the UWB-MIMO channel model.

In this research, some phenomena are revealing and listed as following (1) Propagation distance effect: Capacity is independent of Tx-Rx distance in the LOS/NLOS with heavy clutter. (2) Local scatterers effect: In the environment with local scatterers, the capacity is higher than the environment without local scatterers under LOS and NLOS condition. (3) Antenna spacing effect: The UWB-MIMO capacity increases as the antenna spacing increases and it saturates when the spacing is larger than 0.5 λ . (4)

Antenna array orientation effect: Capacity for perpendicular antenna array is higher than parallel antenna array in LOS condition. But in NLOS condition, capacity is higher for perpendicular antenna array in a guided environment.

(5) Capacity Loss: The relative channel capacity loss due to the effect of high antenna correlation is reduced as SNR increases. (6) From the parameter of S-V model in UWB radio channel model, we can see that Γ decay faster in the LOS condition than in the NLOS condition. (7) The UWB-MIMO channel model has been proved to be effective and accurate.

誌謝

首先，我要對我的指導教授唐震寰老師致上最誠摯的感謝，感謝老師在我碩士兩年的研究生涯中，給于我最細心與凡心的指導與叮嚀，並帶領我一窺無線通訊領域研究的奧妙。

其次，對於波散射與傳播實驗室的學長與同學們也要致上我深深的謝意，他們所給予我在知識上和精神上的啟示與鼓勵以及在實驗量測中的協助，對完成本篇論文有莫大的助益。

最後，要感謝的是我最親愛的父母親由於他們給予我的支持與關懷，使我在人生的過程裡得到最細心的呵護與照顧，讓我在成長與求學的過程中能夠有所依靠。

僅以此篇論文獻給所有關心我的人。

蔡孟勳

國立交通大學，新竹市

中華民國九十四年十月

Table of Contents

Table Captions

Figure Captions

Chapter 1

Introduction

Over the past few decades, there has been rapid development and deployment of cellular phone networks. Recently, there has been development of the so-called wireless LAN technology, as specified in HiperLan/2 for the European standard and IEEE 802.11 for the North American standard. Many of the future wireless services to be provided by the future generation mobile communication systems are likely to be used in low- mobility environments with limited temporal or multipath diversity. This is the reason why most of the communication research that is going on concentrates on realization of indoor environments. The growing demand of increasing the capacity has pushed researches into investigation of space domains, beamforming, use of space diversity/ “smart antennas” and spectral multiplexing. For this reason conventional techniques with a single antenna fails to provide sufficient diversity. Instead multiple antennas give high-data rates and throughputs. Therefore the solution of using multiple antennas at both transmitter and receiver in indoor environment is growing in radio communication systems. Multiple-input multiple-output (MIMO) systems can provide radio channels capable of transferring parallel information within the same bandwidth and increase the attainable capacity [1], [2].

1.1 Paper review

Several effects on capacity and correlation coefficients on MIMO/UWB-MIMO capacity prediction/measurement have been explored. The effect of antenna spacing is reported in the literature [3] that the antenna spacing has little effect on capacity. The effect

of antenna orientation is reported in the literature [4, 8] that receiver antenna array, the one perpendicular to the direct-path direction obtains more capacity than the one parallel to the direct-path direction in a “wave-guiding” environment. The effects of Tx-Rx distance are reported in the literature [5] that for not normalized channel, the channel capacity usually rose when moving from NLOS into LOS since the loss in multipath was more than compensated for by an increase in SNR. The effect of unequal array spacing is reported in the literature [6] that unequal array spacing may obtain the optimum capacity. The effect of correlation of the antenna elements is reported in the literature [7] that correlations of the antenna elements are the limiting factor for the channel capacity. The above mentioned works are summarized in Table 1.

Several effects on UWB radio channel modeling have been explored. Characterization of UWB channels are reported in the literature [9] that present character UWB channels for outdoor office environment in LOS and NLOS cases. Reference [10] indicates that means angles of each cluster were found to be distribution uniformly over all angles. The distribution of arrivals within clusters was approximately Laplacian. In the literature [11] that parameters of S-V model are compared with the parameters presented in the paper by Saleh and Valenzuela. The above mentioned works are summarized in Table 2

Several effects on MIMO/UWB MIMO radio channel modeling have been explored. Reference [12] presents a set of channel models applicable to indoor MIMO WLAN systems. Reference [13] presents a simplified UWB-MIMO channel model that combine IEEE 802.15.3a channel model recommendation and a wideband MIMO channel model structure. In the literature [14] that UWB system is represented by a STDL model and MIMO system is represented by MIMO channel covariance matrix. The above mentioned works are summarized in Table 3.

1.2 Motivation

Recent years have seen the emergence of high data rate, third generation wideband wireless communication standards like wideband code division multiple access (W-CDMA) and UWB radio. Motivated by the ever increasing demand for higher wideband wireless data rates, we consider multiple antenna communication over the UWB wireless channel (UWB-MIMO). The spectral efficiency of UWB-MIMO system could be greatly increased when the channel is deployed in rich multipath condition such as indoor environment, where any two multipath components may have low correlation. Thus to investigate the capacity and correlation properties of the UWB-MIMO radio channel under various propagation and array arrangement will be an interesting and important subject. And few people do research on UWB-MIMO channel model.

1.3 Purpose

In this thesis, we will introduce the capacity and correlation properties of UWB-MIMO channels and analyze the measured UWB-MIMO channel data to investigate the effects of propagation range, local scatterer, antenna array spacing, array orientation and bandwidth. And in order to propose a set of channel models applicable to indoor UWB-MIMO systems. We first present the characterization of UWB channels for indoor environment with above measured data. Then we base on 802.11n channel model to develop the UWB-MIMO channel model.

1.4 Organization

This thesis is composed of 7 chapters as following: In chapter 2, the fundamental theory of UWB-MIMO systems will be introduced. Chapter 3 is the UWB-MIMO channels measurement. We will describe the UWB-MIMO channels measurement system and the measurement environments. In chapter 4, according to the measured data, the capacity,

EDOF, correlation coefficients and capacity loss of UWB-MIMO channel will be defined and calculated. The effects of propagation range, local scatterer, antenna spacing, array orientation and bandwidth effect will be considered. In chapter 5, character UWB channels for indoor environment with above measured data. The Saleh-Valenzuela (S-V) model [19] is used as a basis for our UWB channel model. In chapter 6, we propose a set of channel models applicable to indoor UWB-MIMO systems. The newly developed UWB MIMO channel models are based on the 802.11n channel model [12]. A brief conclusion is provided in Chapter 7.

Table 1 Summary of related works on MIMO/UWB-MIMO capacity prediction and measurement

Ref. No.	Freq. (GHz)	Meas. Sites	Meas. Result	Remarks
[3]	5.1-5.3	In the entrance hall Tx and Rx are 10m apart	Spacing has little effect	Prediction of MIMO
[4]	2.4	Corridor dimensions are (100m×4m×3m) Room dimensions are (10m× 10m×3m)	Array orientation that is perpendicular to the direct-path obtains more capacity in the corridor	Prediction of MIMO
[5]	2.43	Corridor	Capacity decreases with distance increases	Measurement of MIMO
[6]	5.8	Indoor environment (virtual transmitter and receiver antenna array)	Unequal array spacing may obtain the optimum capacity	Measurement of MIMO
[7]	5.14 -5.26	Indoor office	The correlation of the antenna elements are the limiting factor for the channel capacity.	Measurement of MIMO
[8]	5.225– 5.725	Corridor dimensions are 100m×2m	For a deterministic channel, with a strong LOS and small angular spread, the horizontal orientation of the receiver antenna array can make a significant difference in channel capacity gain.	Measurement of UWB-MIMO

Table 2 Summary of related works on UWB radio channel modeling

Ref. No.	Freq. (GHz)	Meas. Sites	Meas. Result
[9]	3 - 6	Outdoor office environment	Present a characterization of UWB channels for outdoor office environment in LOS and NLOS cases.
[10]	6.75 - 7.25	Indoor environment in two building	The mean angles of each cluster were found to be distribution uniformly over all angles. The distribution of arrivals within clusters was approximately Laplacian.
[11]		Indoor office environment Indoor laboratory environment	The parameters of S-V model in this paper are compared with the parameters presented in the paper by Saleh and Valenzuela.

Table 3 Summary of related works on MIMO/UWB MIMO radio channel modeling

Ref. No.	Freq. (GHz)	Analyzed results	Remarks
[12]	2.4 5.25	Present a set of channel models applicable to indoor MIMO WLAN systems.	MIMO
[13]	4 - 10	A simplified UWB-MIMO channel model that combines IEEE 802.15.3a channel model recommendation (S-V model) and a wideband MIMO channel model structure.	UWB MIMO
[14]		UWB system is represented by a STDL model and MIMO system is represented by MIMO channel covariance matrix	UWB MIMO

Chapter 2

Fundamental Theory of UWB-MIMO Systems

It is well known that using antenna arrays at both transmitter and receiver over a multiple-input–multiple-output (MIMO) channel can provide a very high channel capacity as long as the environment has sufficiently rich scattering. Under these circumstances, the channel matrix elements have low correlation and the channel realizations are high rank, leading to a substantial increase in channel capacity.

In this chapter we will introduce the fundamental theory of UWB-MIMO systems, complex spatial correlation coefficient and EDOF (Effective Degrees of Freedom).

2.1 Generalized UWB-MIMO capacity formula

Consider a UWB-MIMO system with M transmits elements and N receives elements. The baseband input-output relationship is given by

$$\vec{y}(\tau) = \vec{H}(\tau) \times \vec{s}(\tau) + \vec{n}(\tau)$$

where $\vec{s}(\tau)$ is the transmitted signal, $\vec{y}(\tau)$ is the receiver signal, $\vec{n}(\tau)$ is AWGN (Additive White Gaussian Noise) and $\times$ denotes convolution. Each element of the channel impulse response matrix $\vec{H}(\tau)$ is the impulse response from a transmit antenna to a receiver antenna.

When the transmitted power is equally allocated to each transmit element and frequency subchannel, the UWB-MIMO channel capacity can be expressed as [17], [31]

$$C = \frac{1}{W}\int_{W} \log_2 \det\left(\mathrm{I}_{n_R} + \frac{\rho}{n_T} \mathrm{H}(f)\mathrm{H}^*(f) \right) df \qquad \text{bits/s/Hz} \qquad (2\text{-}1)$$

where n_T and n_R are the numbers of Tx and Rx antenna array elements, respectively, and W is the overall bandwidth of the MIMO channel, $\mathrm{H}(f)$ is the normalized frequency response matrix of each narrow-band subchannel, * is the complex conjugate, and ρ is the average SNR at each receiver branch over the entire bandwidth. Since the measured UWB-MIMO matrices include the pathloss, we have to do a normalization to set the average receiver SNR to a specific value. Here, we normalize the frequency response of every narrow-band subchannel using a common factor such that

$$\int_{W} E\left(\|\mathrm{H}(f)\|_F^2 \right) df = W n_T n_R$$

We also write capacity formula into another form [10]

$$C_i = \frac{1}{N_f}\sum_{f}^{N_f} \log_2 \left(\det\left(I_{N_R} + \frac{\rho}{n_T} H_{i,f} H_{i,f}^* \right) \right) \qquad \text{bits/s/Hz} \qquad (2\text{-}2)$$

where N_f is frequency components and *i* is the time or snapshot index.

The normalization factor for each UWB-MIMO measurement snapshot T_i (*i* is the time or snapshot index) was calculated separately. This removed the effect of large-scale spatial fading, which can be significant for dynamic measurements, and ensured that only the small-scale: spatial fading was observed. T_i has dimensions of $n_R \times n_T \times N_f$, where n_R, n_T, N_f are the number of receive antennas, transmit antennas and frequency components respectively. Each 4x4 measured channel snapshot had dimensions of (4×4×801), thus providing a sufficient number of independent samples for normalization. The normalized UWB-MIMO channel H_i was calculated from (2-3) and **(**2-4**),** where $\hat{\eta}_k$ is the normalization factor estimate.

$$H_i = \frac{T_i}{\hat{\eta}_k} \tag{2-3}$$

$$\hat{\eta}_k^{\,2} = \frac{1}{n_R n_T N_f} \sum_{f=1}^{N_f} \sum_{j=1}^{n_R} \sum_{k=1}^{n_T} \left| T_{i,f,j,k} \right|^2 \tag{2-4}$$

The goal of channel normalization is usually to scale the channel response so that the expectation of its power is unity. We refer to this as *unity-gain* normalization.

2.2 Complex Spatial Correlation Coefficient

In addition to capacity, we also considered the correlation at both transmit and receive side. To estimate the receive and transmit correlation matrix we let h_{ij} be the channel complex gain between j-th Tx element and i-th Rx element. The complex correlation coefficient between h_{ij} and h_{kl} is given as [21]

$$\rho(a,b) = \frac{E[ab^*] - E[a]E[b^*]}{\sqrt{E[|a|^2 - |E[a]|^2]E[|b|^2 - |E[b]|^2]}}$$

where * denotes the complex conjugate operation and $\boldsymbol{a} = \boldsymbol{h_{ij}}$ and $\boldsymbol{b} = \boldsymbol{h_{kl}}$. The complex correlation coefficient is a complex number that is less than unity in absolute value. In the following figures we will only present its absolute value. Also, it is assumed that all antenna elements in the two arrays have the same polarization and the same radiation pattern. To describe the propagation environments around Tx and Rx, the correlation coefficients of Tx and Rx are explored and given by [21], respectively,

$$\rho_{Tx} = \rho(h_{ij}, h_{il}) \tag{2-5}$$

$$\rho_{Rx} = \rho(h_{ij}, h_{kj}) \tag{2-6}$$

Receiver correlation describes the local scattering around the receivers, whereas transmitter correlation describes the correlation of the transmitted signals as seen at the

receiver and does not provide insight into the scattering of the environment close to the transmitter array.

It is noted that ρ_{Tx} and ρ_{Rx} are first averaged over the index elements (j, l) or (I, k) then over the element indices i (receiving elements) and j (transmitting elements) respectively.

2.3 Effective Degrees of Freedom (EDOF)

The notion of multipath richness is less formal than capacity and there are several potential measures that could be used. Here, the concept of Effective Degrees of Freedom (EDOF) [2] will be used. This measure is based on the fact that for an $N \times N$ channel with rich multipath (fully decorrelated channel), a capacity increase of N bits is obtained when doubling the transmitted power. A correlated channel, i.e. a channel with fewer multipaths, will exhibit a smaller capacity increase. Hence, a convenient measure of the multipath richness is the slope of the capacity curve defined as

$$EDOF = \frac{\partial}{\partial \delta} C\left(2^{\delta} \rho\right)\Big|_{\delta=0} \tag{2-7}$$

By rewriting the capacity expression in (2-1) [9] as

$$C(\rho) = \sum_{k=1}^{\min\{n_T, n_R\}} \log\left[1 + \frac{\rho}{n_T} \lambda_k\right] \tag{2-8}$$

Where $\sqrt{\lambda_k}$ denotes the singular values of the normalized channel matrix it is straightforward to calculate the derivative in (2-7)

$$\frac{\partial}{\partial \delta} C\left(2^{\delta} \rho\right) = \sum_{k=1}^{\min\{n_T, n_R\}} \frac{1}{1 + \frac{n_T}{2^{\delta} \rho \lambda_k}} \tag{2-9}$$

The EDOF is then obtained as

$$EDOF = \sum_{k=1}^{\min\{n_T, n_R\}} \frac{1}{1 + \frac{n_T}{\lambda_k \ \rho}} \tag{2-10}$$

Note that the EDOF is a real number in $[0, \min\{n_T, n_R\}]$. A LOS channel with one dominant propagation path will yield an EDOF close to one while a rich NLOS channel will be close to $\min\{n_T, n_R\}$. For channels in between these, the EDOF will essentially be the minimum of the number of transmit and receive antennas or the number of propagation paths with non-negligible strength [33]. Unfortunately, the EDOF measure depends on the SNR since the number of independent transmission channels that rise above the noise floor depends on the SNR. In this paper the EDOF will be calculated assuming a medium SNR of 10dB.

Chapter 3

Measurement System and Environment

In a typical indoor environment, due to reflection, refraction and scattering of radio waves by structures inside a building, the transmitted signal most often reaches the receiver by more than one path, resulting in a phenomenon known as multipath fading. In UWB pulse transmission, the effect is to produce a series of delayed and attenuated pulses (echoes) for each transmitted pulse.

In order to fulfill the requirement of higher data rates and capacities for future indoor wireless communications, numerous research programs are now underway and focused on evaluating and characterizing the wireless radio channel so that proper radio architectures with omni-directional UWB antennas on MIMO can be designed and implemented efficiently. This requires obtaining the channel characteristics in different environments, the UWB-MIMO channel measurement methods are proposed for analyzing each composition of multipath response. Later we will classify the propagation scenarios into following six categories:

1. LOS (Line-of-Sight) with light and heavy clutter (scenarios I and II).
2. NLOS (Non-Line-of Sight) with light and heavy clutter (scenarios III and IV).
3. LOS and NLOS in a guided environment such as corridors (scenarios V and VI).

3.1 Measurement System and Setup

In order to obtain the channel characteristics, the UWB channel measurement is performed to analyze the MPCs. An Agilent 8719ET Vector Network Analyzer (VNA) is

exploited to measure the channel response between two ends. The transmitted signal is sent from the VNA to the transmitting antenna through a low-loss 10-m coaxial cable.

For our measurement operation, we use a pair of omni-directional UWB antennas by Electro-Metrics (EM-6865), which frequency range is 2-18 GHz and antenna gain is 0dBi. The signal from the receiving antenna is through a preamplifier (with a gain of 30 dB) via a low-loss 30-m coaxial cable and then returned to port 2 of the VNA. For UWB-MIMO application, the swept frequency band is from 3.5GHz to 4.5GHz (1GHz of frequency span). With 1.25MHz steps corresponding to 801 points, we would be able to detect multipath with a time delay up to 800ns. Besides the network analyzer, the time-domain channel response can be obtained by taking the inverse Fourier transform (IFFT) of the frequency-domain channel response. Table 4 lists the main parameters in the measurement.

Because Agilent 8719ET is a SISO system with 2 omni directional antennas at both ends, we have simulated the 4x4 MIMO channels by moving the Tx and Rx to the ULA (Uniform Linear Array) fixed points. During the measurement, both the Rx and Tx antennas are at a height of 1.5m above the ground. And the measurement system that we used is shown in Figure 3-1, 3-2, 3-3.

Table 4 The main parameters in the measurement

Parameter	**Value**
Frequency band	3.5GHz to 4.5GHz
Bandwidth (frequency span)	1GHz
Number of points over the band	801
Transmitted power	10dBm
Preamplifier gain	30dB
Antenna gain	0dBi

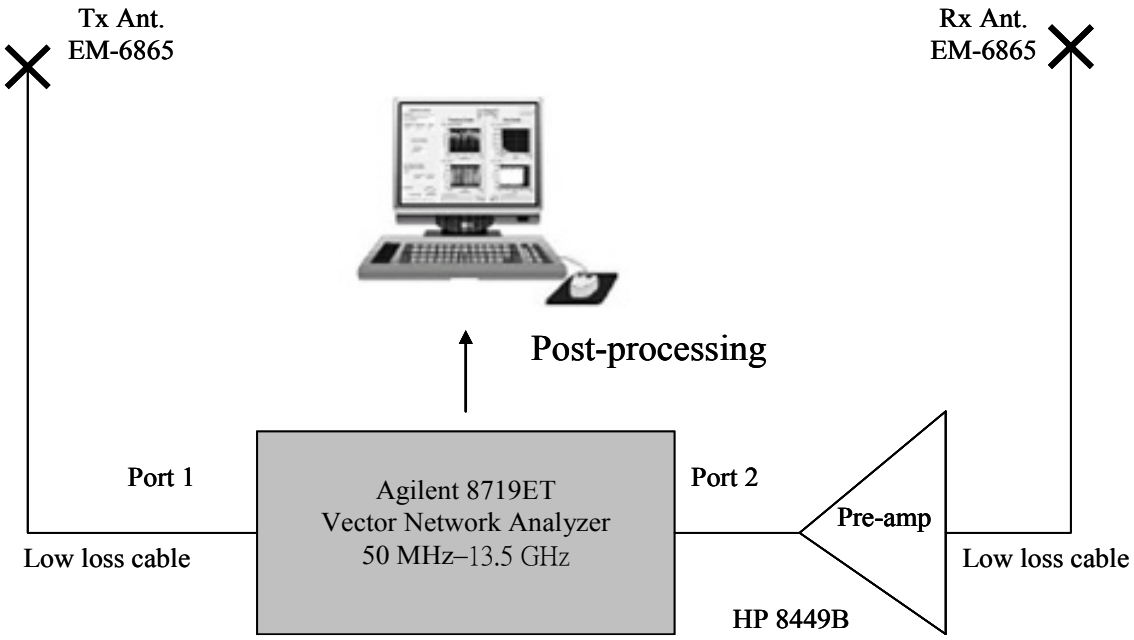

Fig. 3-1 Block digram of the measured system

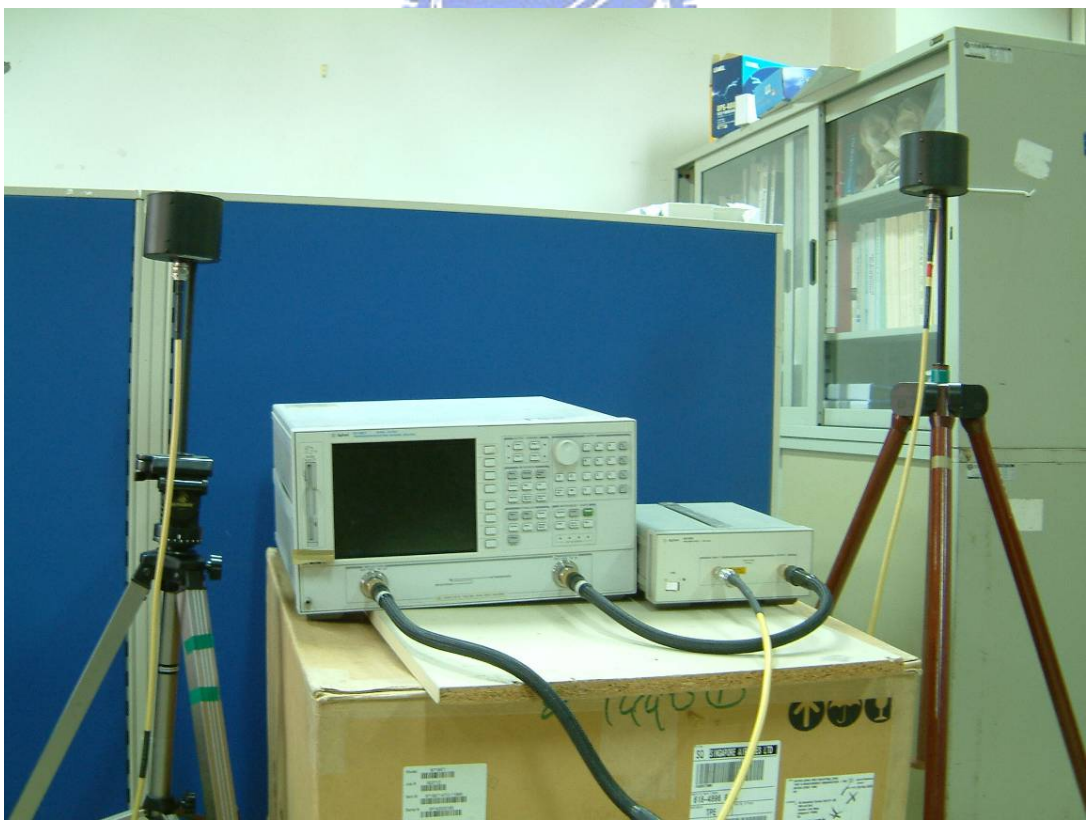

Fig. 3-2 A photo of the frequency domain channel sounding system

Fig. 3-3 A photo of the UWB antenna.

3.2 The Description of Measurement Environment

The measurement was performed in 1^{st} floor (site A), 2^{nd} floor (site B and C), 7^{th} floor (site E), and 8^{th} floor (site F) of the Microelectronics and Information System Research Center (MISRC) and 2^{nd} floor (site D) of the 4^{th} Engineering Building at the National Chiao-Tung University, Hsinchu, Taiwan. The layout is shown in Fig. 3-4.

In order to compare the difference of capacity, EDOF and correlation for varied Tx-Rx distance in the scenarios I, II, III and IV, we do some measurement at site A, B and C. At site A, path 2 is measured at 1^{nd} floor of the MISRC and NLOS is always existed in path 2. At site B, path 1 is measured at 2^{nd} floor of the MISRC and LOS is always existed in path 1. At site C, both path 3 and path 4 are measured at Room 213 of the MISRC. And LOS is always existed in path 3. For instead of LOS, the NLOS exists in path 4. In the path 1, 2, 3, and 4, we take the samples when the Tx antenna array moves every 1m.

In order to analyze how the local scatterer affects the UWB-MIMO capacity and correlation in the scenarios I, II, III and IV, we carry out the measurement in site D. The Room 202 and 203 are all enclosed with concrete walls and wooden doors. All of them are clustered with wooden chairs. During the measurement, we don't move these chairs to stand for the environment with local scatterers (scenarios II/IV). And then we move these chairs far away Tx, Rx to stand for the environment without local scatterers (scenarios I/III).

We adjust the element spacing of the virtual antenna arrays to investigate how the capacity varies is with different antenna spacing in the scenarios I, II, III and IV. At P1, P2, P3, P4, P5 and P6, both Tx and Rx antenna spacing is changed from 0.1λ to 2.0λ. In order to know the difference between LOS and NLOS condition, we measure at P1, P3 & P5 under the LOS condition, and P2, P4 & P6 under NLOS condition.

In order to compare with the difference of varied antenna array orientation in the scenarios II, IV, V and VI, we do some measurement at site E and site F. For each transmit antenna position, the complex transfer functions were recorded for 10 receive antenna positions, 5 positions with the broadside of the virtual antenna perpendicular to the LOS (orientation I) and 5 positions with the broadside parallel to the LOS (orientation II). The array broadside orientation is shown in Fig. 3-5.

The frequency response data have been exploited to analyze the UWB-MIMO channel characteristics. We observe the frequency response between 3.5GHz to 4.5GHz with 801 sweep points. Detailed measurement sites are shown in Table 5.

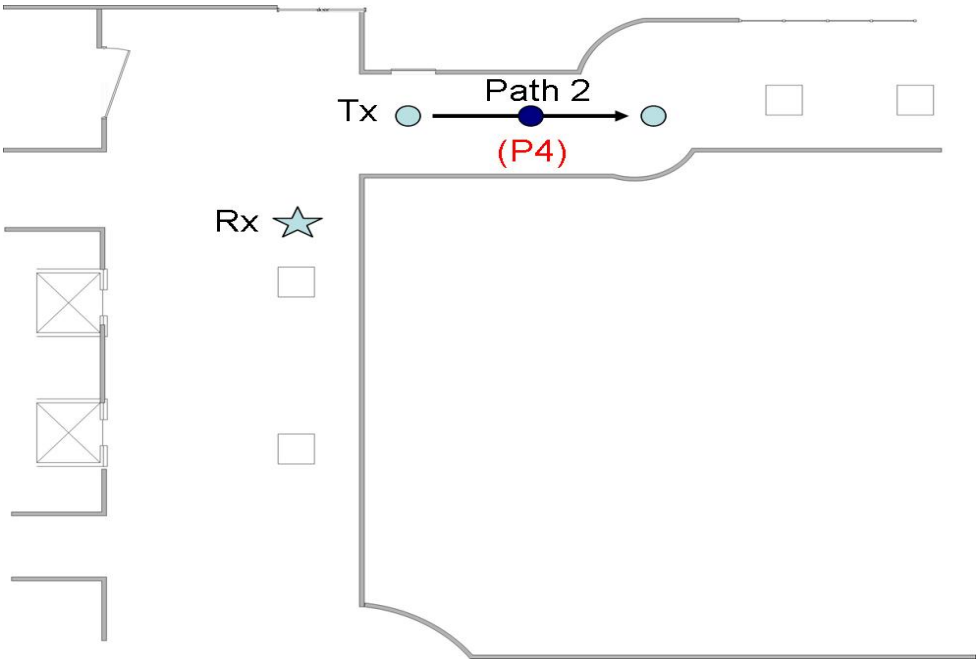

Fig. 3-4 (a) Site A: 1^{st} floor layout of the Microelectronics and Information System Research Center (MISRC)

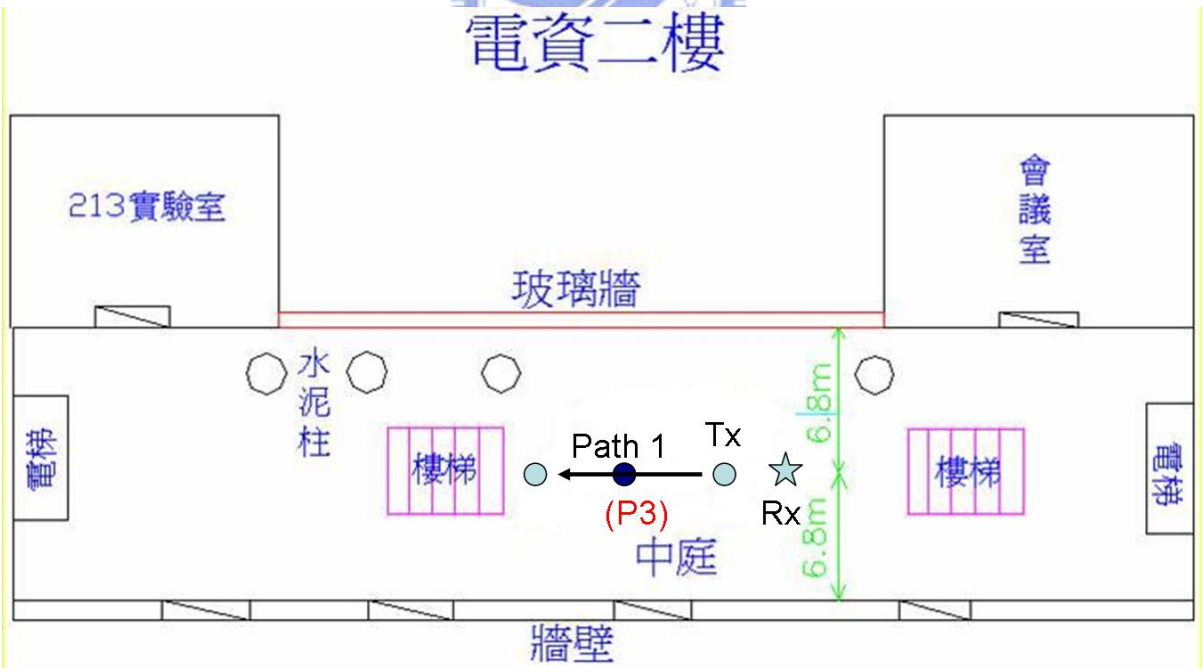

Fig. 3-4 (b) Site B: 2^{nd} floor layout of the MISRC

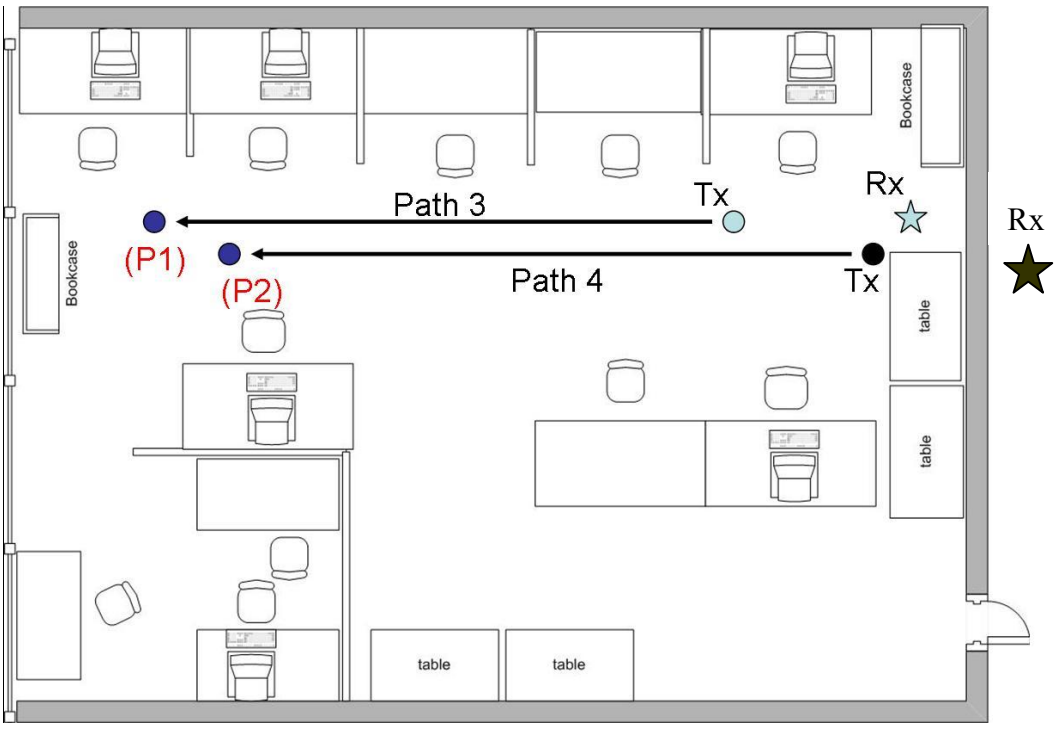

Fig. 3-4 (c) Site C: Lab 213 layout of the MISRC

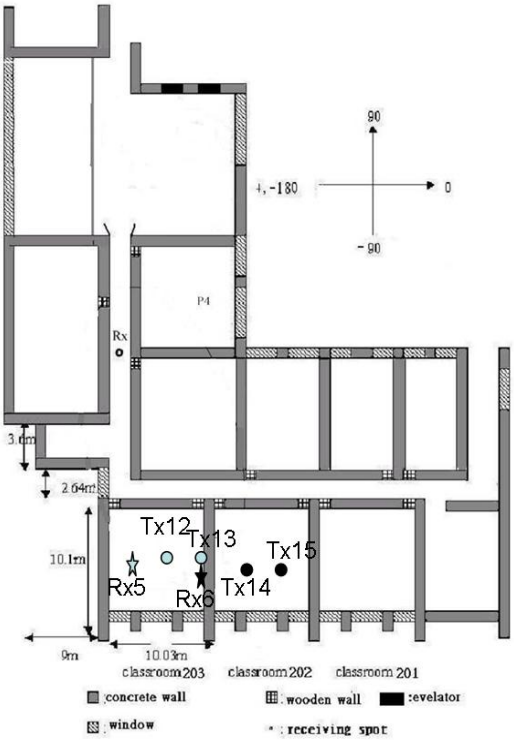

Fig. 3-4 (d) Site D: 2^{nd} floor layout of the 4th Engineering Building

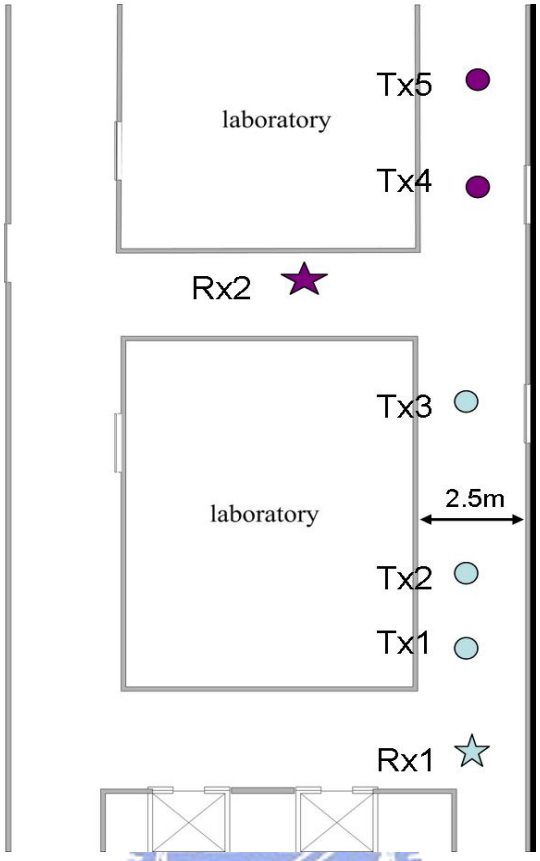

Fig. 3-4 (e) Site E: 7^{th} floor layout of the MISRC

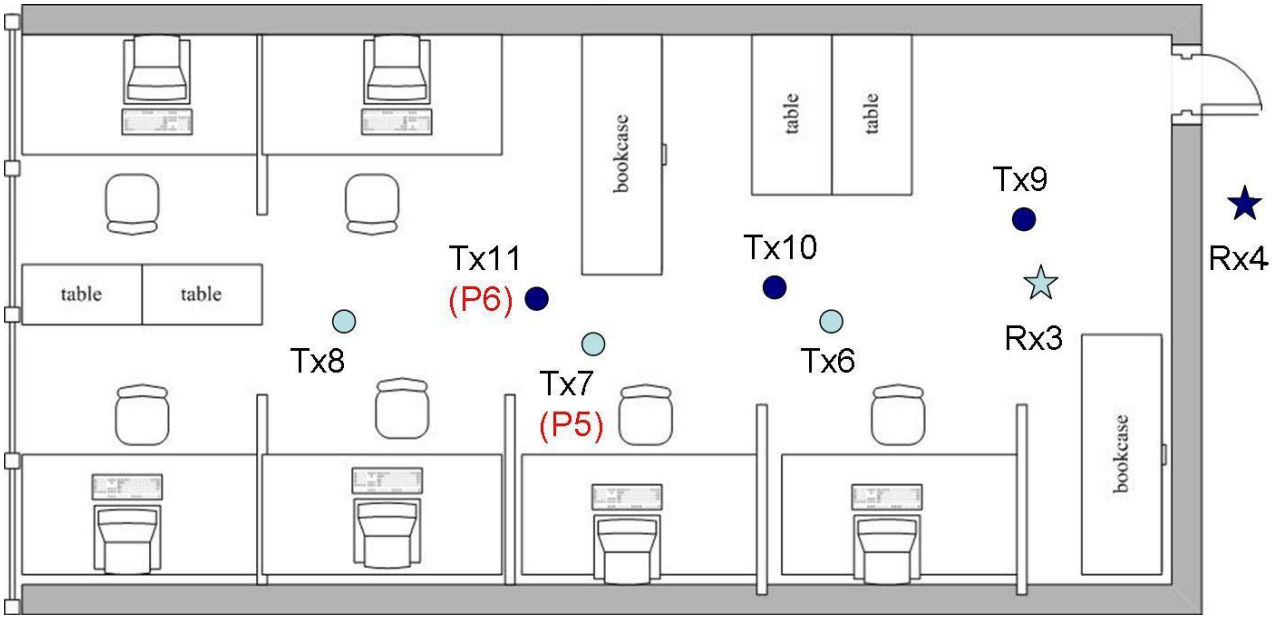

Fig. 3-4 (f) Site F: Lab 810 layout of the MISRC

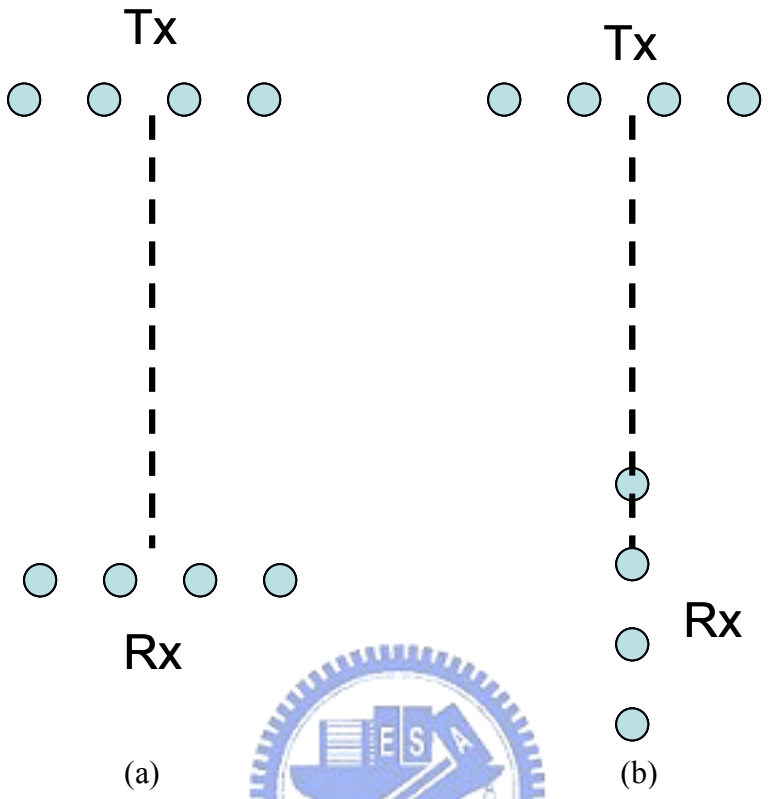

Fig. 3-5 Receiver antenna broadside (a) perpendicular (orientation I)

(b) parallel to the direct path (orientation II)

Table 5 Measurement sites

Location	Distance (Tx-Rx)	Measurement Scenarios
Site A (1st floor of MISRC)	Path 2=4~18m (P4=11m)	Scenario III
Site B (2nd floor of MISRC)	Path 1=2~15m (P3=8m)	Scenario I
Site C (Lab 213 of the MISRC)	Path 3=2~8m (P1=8m)	Scenario II
	Path 4=3~11m (P2=11m)	Scenario IV
Site D (Room 202, 203 of the 4th Engineering Building)	Tx12-Rx5=3m Tx13-Rx5=7m	Scenarios I/II
	Tx14-Rx6=3m Tx15-Rx6=7m	Scenarios III/IV
Site E (7th floor corridor of the MISRC)	Tx1-Rx1=3m Tx2-Rx1=7m Tx3-Rx1=13m	Scenario V
	Tx4-Rx2=13m Tx5-Rx2=17m	Scenario VI
Site F (Lab 810 of the MISRC)	Tx6-Rx3=3m Tx7-Rx3=7m (P5) Tx8-Rx3=10m	Scenario II
	Tx9-Rx4=3m Tx10-Rx4=7m Tx11-Rx4=10m (P6)	Scenario IV

Chapter 4

Propagation, Array Arrangement and Bandwidth on UWB-MIMO Capacity and Channel Correlations

To investigate the capacity and correlation properties of the UWB-MIMO channel under various propagation, array arrangement and bandwidth will be an interesting and important subject. In this chapter, the effects of propagation range, local scatterers, antenna spacing, array orientation and bandwidth on the UWB-MIMO capacity, EDOF and correlation are investigated through the measurement.

4.1 UWB-MIMO capacity, EDOF and correlations evaluation

From Eq. (2-2), the 4×4 MIMO capacity is given by

$$C_i = \frac{1}{801}\sum_{f=1}^{801}\log_2\left(\det\left(\mathrm{I}_4 + \frac{\rho}{4}\mathrm{H}_i(f)\mathrm{H}_i^{*}(f)\right)\right) \quad \text{bits/s/Hz}$$

$$\mathrm{H}_i(f) = \frac{\mathrm{T}_i(f)}{\hat{\eta}_k}$$

$$\hat{\eta}_k^{\,2} = \frac{1}{4\times 4\times 801}\sum_{f=1}^{N_f}\sum_{j=1}^{n_R}\sum_{k=1}^{n_T}\left|\mathrm{T}_{i,f,j,k}\right|^2$$

The capacity is calculated with $\rho = 10dB$ and the measured 4×4 UWB-MIMO channel matrix, T_i *(i* is the time or snapshot index), which is realized through the measurement by Agilent 8719 ET vector network analyzer. The normalized UWB

channel H_i was calculated from (2-3) and **(**2-4**),** where $\hat{\eta}_k$ is the normalization factor estimate.

From Eq. (2-10), the EDOF is then obtained as

$$EDOF = \sum_{k=1}^{\min\{n_T, n_R\}} \frac{1}{1+\frac{4}{\lambda_k \rho}}$$

And from Eq. (2-5) (2-6), the spatial correlation coefficient at Tx, Rx between elements are calculated.

4.2 Propagation Range Effect (Scenarios I/II/III/IV)

To investigate the propagation range effect on capacity, EDOF and correlations, we perform the measurement for a (4×4) UWB-MIMO system in two kinds of indoor environments: one in the lobby with light clutter (site A and site B) and another in the laboratory with heavy clutter (site C). We also consider the LOS and NLOS situation in two environments (scenarios I/II/III/IV). During the measurement, the antenna array broadside orientation direction is always perpendicular to the direct-path direction.

4.2.1 LOS with light/heavy clutter (scenarios I/II)

From Fig. 4-1 to fig. 4-2 illustrate the capacity, EDOF and correlations versus Tx-Rx distances in the LOS condition (scenarios I/II). By the chart of Fig. 4-1, we can find that in the scenario I, when Tx-Rx distance is in near distance, the capacity will be lower. But when distance is added to 10m, the capacity will not be changed obviously for distance increase. The reason is that because the Tx and Rx is very close, the correlations are relative higher at 1m, 2m and 3m (noted from Fig.4-1 (c) (d)). The LOS clutter strongly raises the correlation and then will cause the capacity reduced. In Fig. 4-1 (b) (EDOF vs. distance) can find the same tread as Fig. 4-1 (a).

From fig. 4-2, we can find that capacity, EDOF and correlations are all similar for

various distances in the scenario II. The reason is that there are heavy clutters in the laboratory so that when the Tx-Rx is in near distance, multipath will increase (compare with the scenario I), then correlations are not as high as the scenario II.

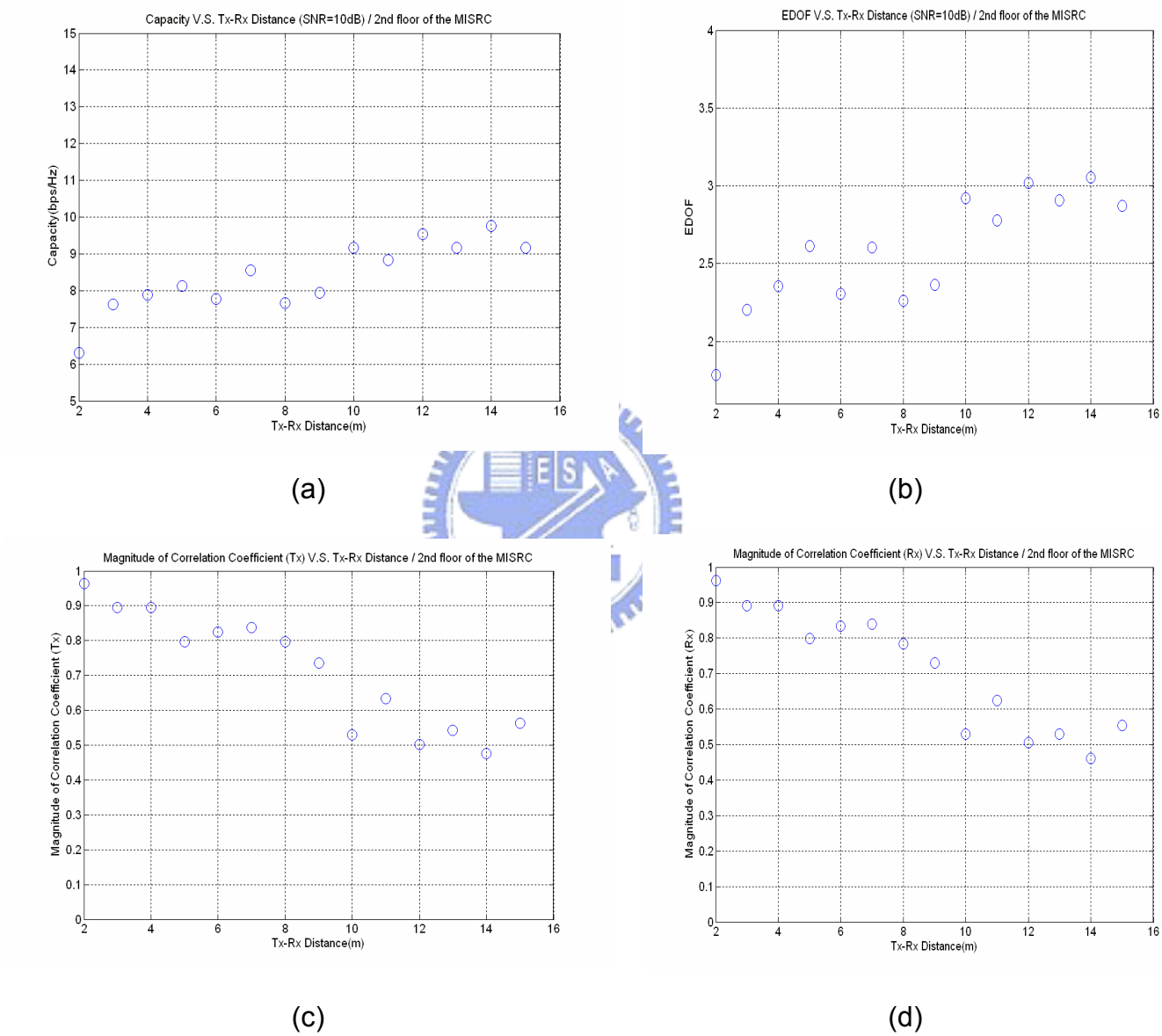

Fig 4-1 Measured results at site B (in LOS condition in scenario I)

(a) Capacity versus distance; (b)EDOF versus distance;

(c) ρ_{Tx} versus distance; (d) ρ_{Rx} versus distance

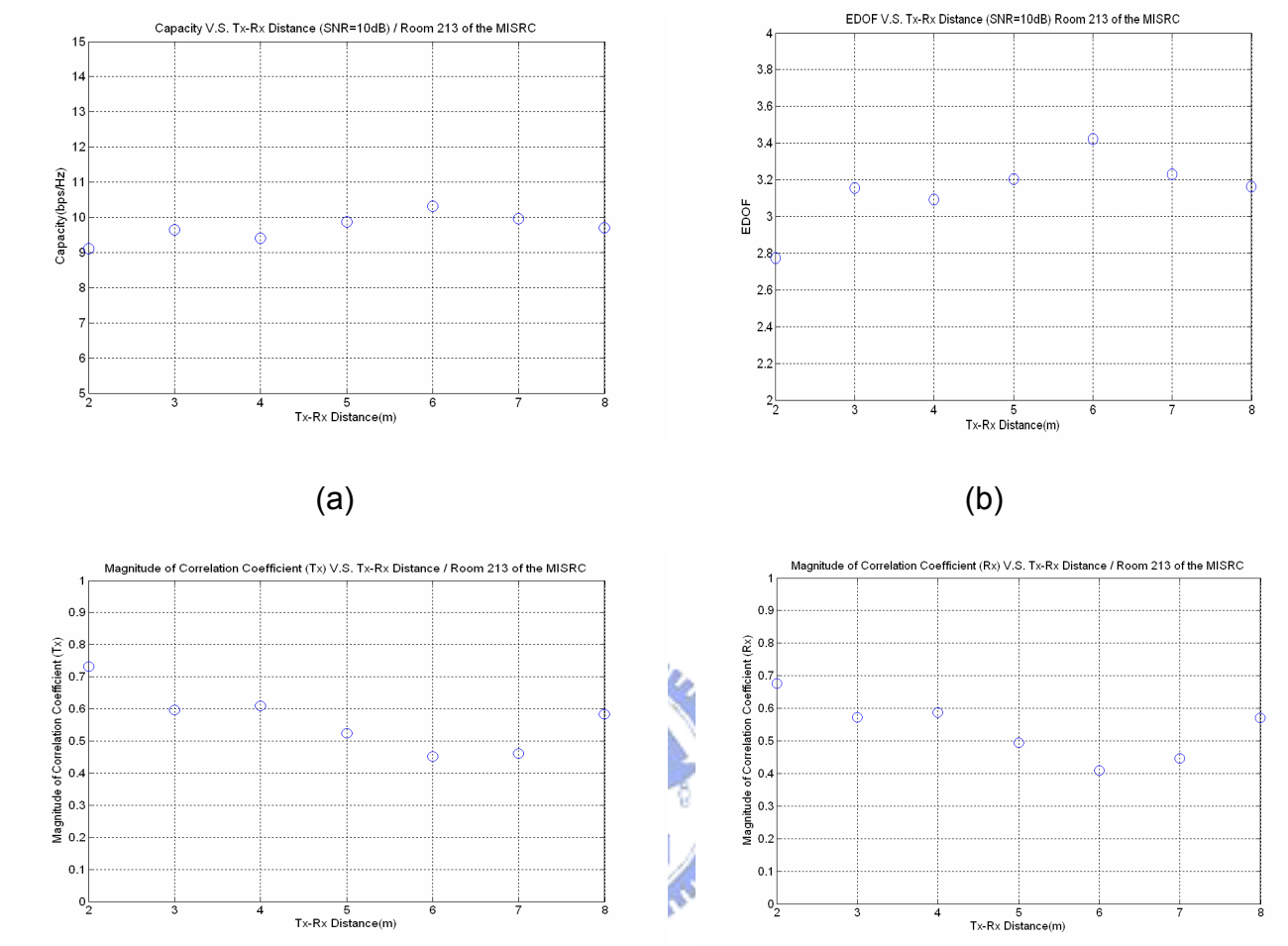

Fig 4-2 Measured results at site C (in LOS condition in scenario II)

(a) Capacity versus distance; (b) EDOF versus distance;

(c) ρ_{Tx} versus distance; (d) ρ_{Rx} versus distance;

4.2.2 NLOS with light/heavy clutter (scenarios III/IV)

Fig. 4-3, 4-4 illustrates the capacity, EDOF and correlations versus Tx-Rx distances in NLOS condition (scenarios III/IV). The main difference of Figs.4-1 (site B), 4-2 (site C) and Figs. 4-3 (site A), 4-4 (site C) is that there are many scatterers in the site C (compare with site A/B).

By the chart of Fig. 4-3, we note that in the near distance, there is not a great effect on distance change to capacity, but when distance is during 16~18m, the capacity is low. We can find the reason out in the LAYOUT chart (Fig. 3-5(a)). As Tx-Rx distance is in 16~18m, Tx enter to a wide space and the multipath which RX received is reduced, so that the correlation coefficient is increase and then capacity decreased. The chart of Figs.4-3(c) (d) is the correlation coefficient for Tx, Rx and from the chart we can find that when Tx-Rx distance is in 16-18m, the correlation coefficient is higher.

From fig. 4-4, we can find that capacity, EDOF and correlations are all similar for various distances in the scenario IV. The reason is same with situation II.

Due to above results, we can conjecture that capacity is dependent of Tx-Rx distance in LOS with light clutter, i.e. capacity is lower when Tx-Rx distance in small AS (Angular Spread) of AOA/AOD. But capacity is independent of Tx-Rx distance in the environment with heavy clutter, i.e. capacity is similar for any Tx-Rx distance when AS of AOA/AOD is large.

In addition, to compare Figs.4-1, 4-2, 4-3 and 4-4, we also can find that the capacity is higher under the environment that has scatterers around. With this phenomenon, we have a further discussion in the next section.

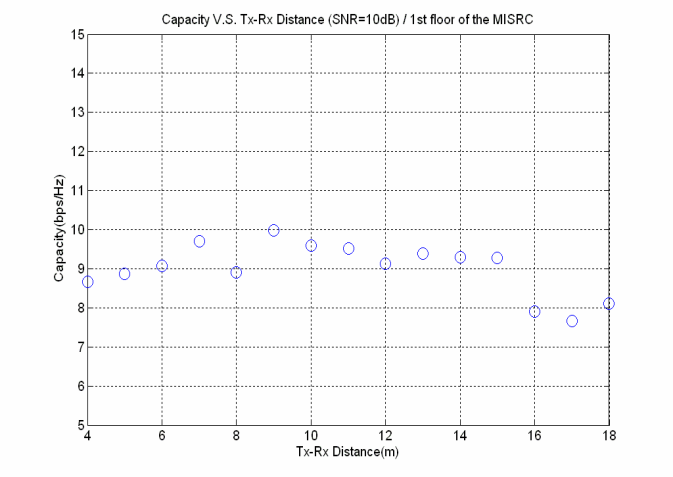

(a)

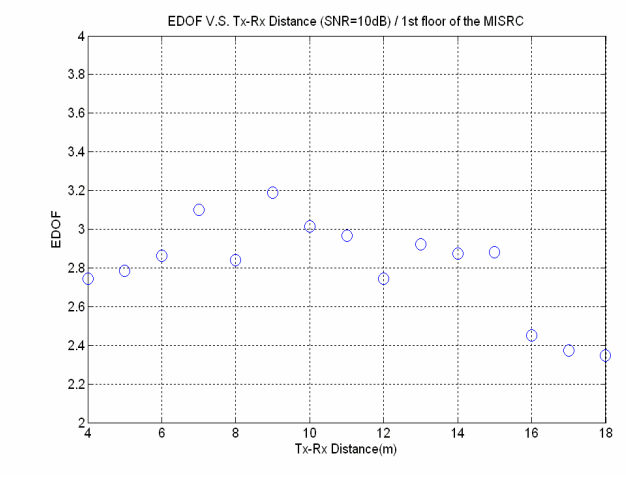

(b)

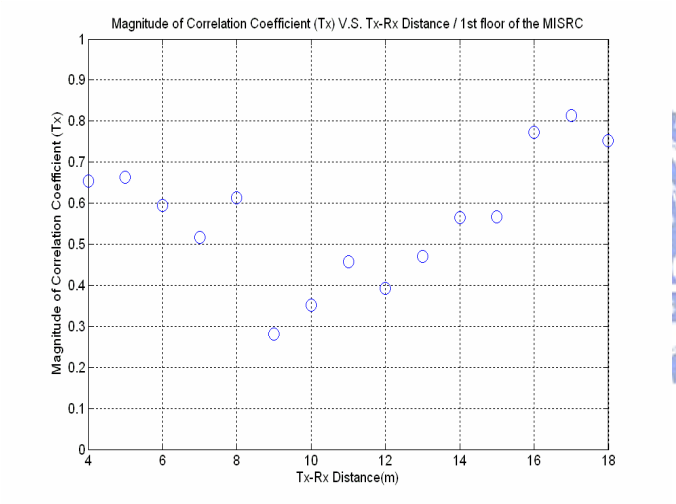

(c)

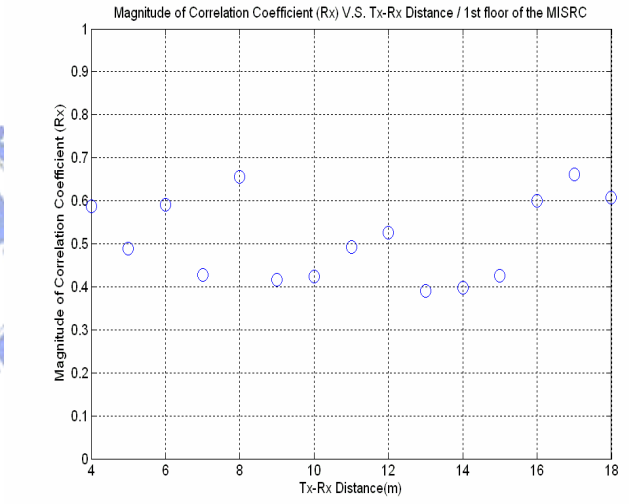

(d)

Fig 4-3 Measured results at site A (in NLOS condition in scenario III)

(a) Capacity versus distance; (b) EDOF versus distance;

(c) ρ_{Tx} versus distance; (d) ρ_{Rx} versus distance

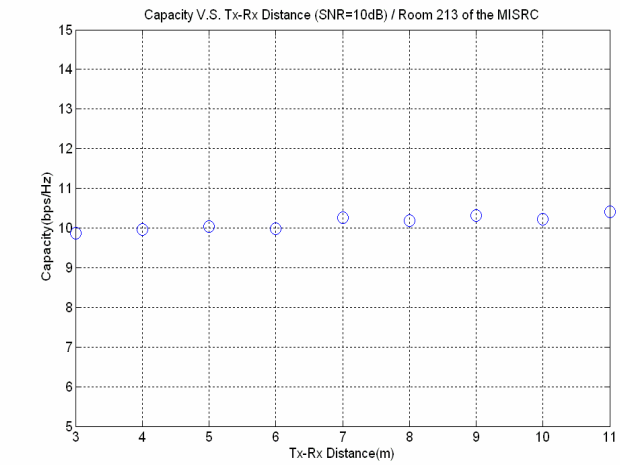

(a)

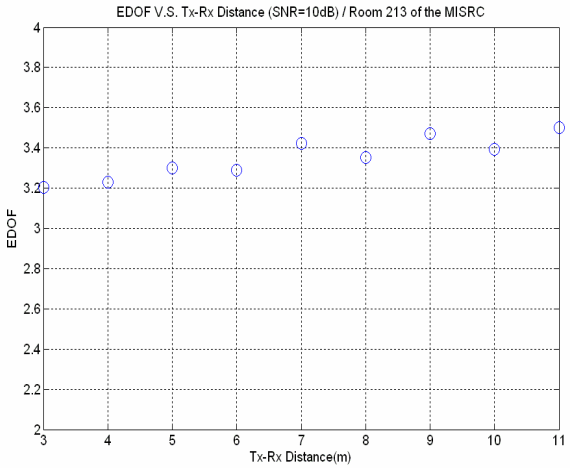

(b)

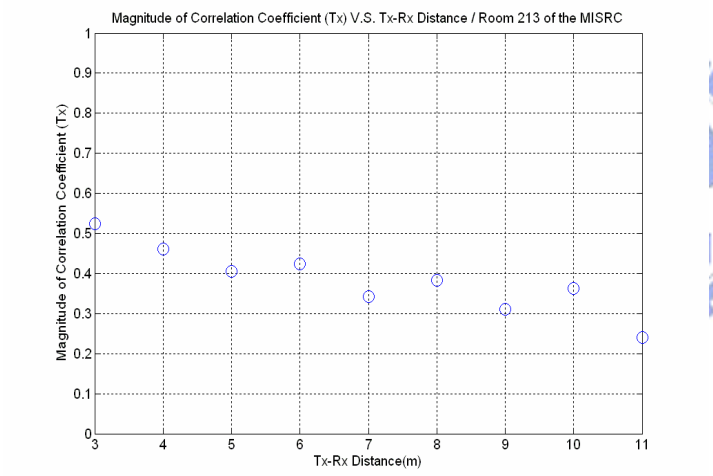

(c)

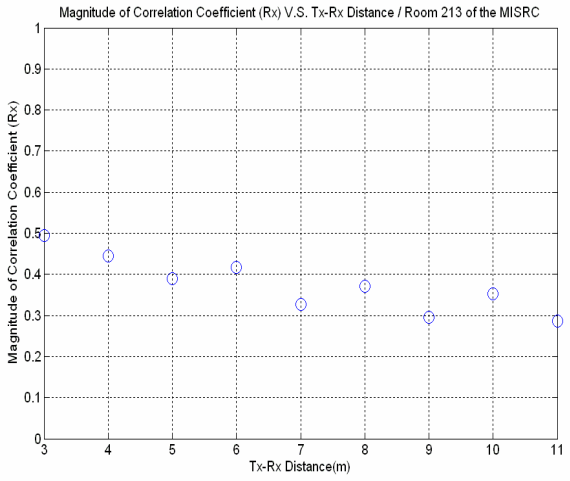

(d)

Fig 4-4 Measured results at site C (in NLOS condition in scenario Ⅳ)

(a) Capacity versus distance; (b) EDOF versus distance;

(c) ρ_{Tx} versus distance; (d) ρ_{Rx} versus distance

4.3 Local Scatterer Effect (Scenarios I/II/III/IV)

In this section, we analyze that how the local scatterer affects the UWB-MIMO capacity and correlation. In the first, we carry out the measurement in the classroom (site D) and consider the LOS and NLOS conditions (scenarios I/II/III/IV). During the measurement, the antenna broadside direction is perpendicular to the direct path direction. The antenna spacing has 0.25, 0.5, and 1 wavelength.

Fig. 4-5 and fig. 4-6 show the capacity and correlations at two kinds of Tx-Rx distance under LOS condition (scenarios I/II). By the chart of fig.4-5(a), we can find that in the environment with local scatterers, the capacity is higher than the environment without local scatterers under any antenna spacing. And the same tread can be found as well in fig. 4-6(a). The reason is that the local scatterer reflect more multipath, and more multipath result in low correlation coefficient (noted from fig.4-5(b)(c), fig. 4-6(b)(c)) and then obtain higher capacity.

The measured result under NLOS condition (scenarios III/IV) is showed in fig. 4-7 and fig. 4-8. We also find the similar outcome as the aforesaid conclusion. So we can conjecture that the environment with heavy clutter will have higher capacity than with light clutter in LOS and NLOS condition.

Furthermore, capacity will be lower when antenna spacing is smaller than 0.5 wavelengths after compare above measured results. Because of this phenomenon, we take the further research in next section.

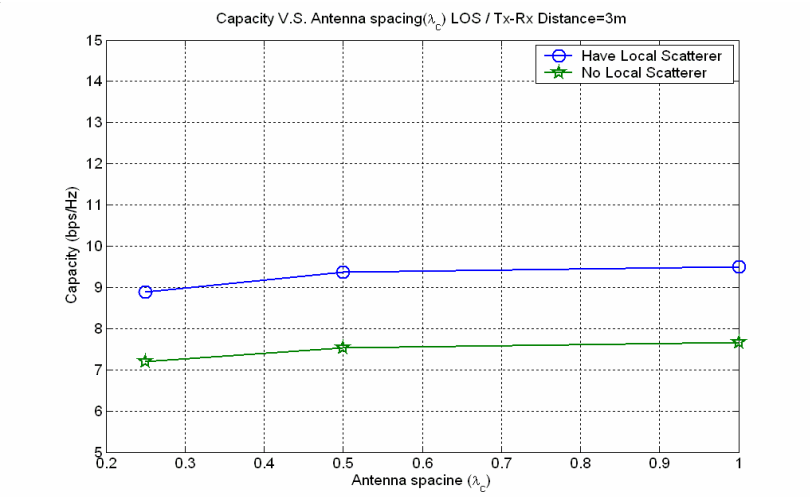

(a)

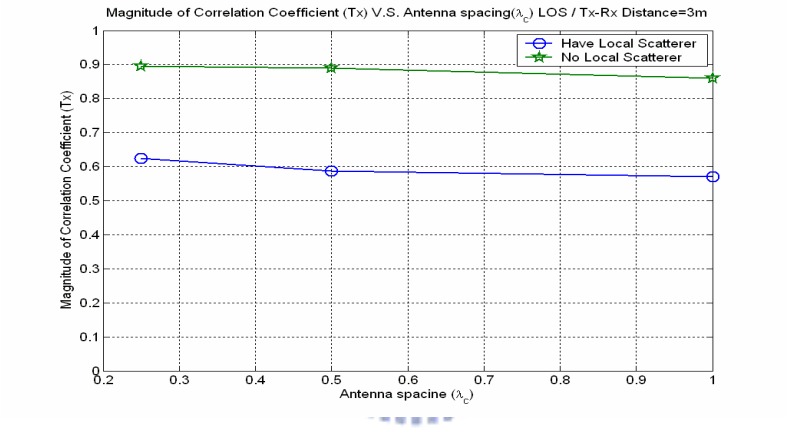

(b)

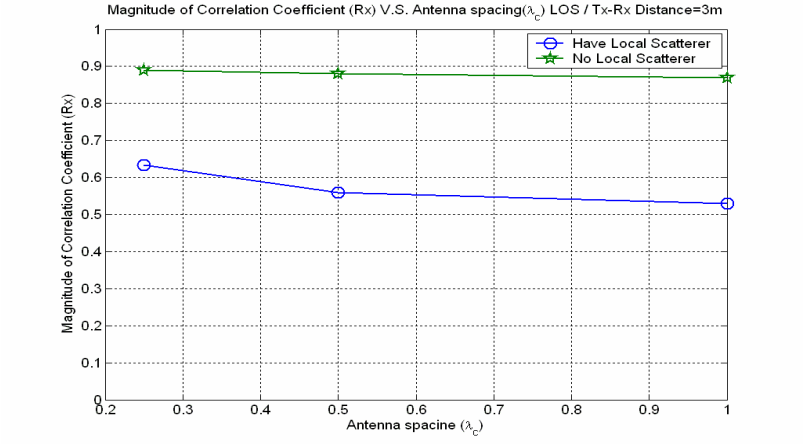

(c)

Fig. 4-5 Local Scatterers discussion under LOS condition in site D (scenarios I/II)

(a) Capacity (b) ρ_{Tx} (c) ρ_{Rx} versus antenna spacing at Tx-Rx Distance=3m

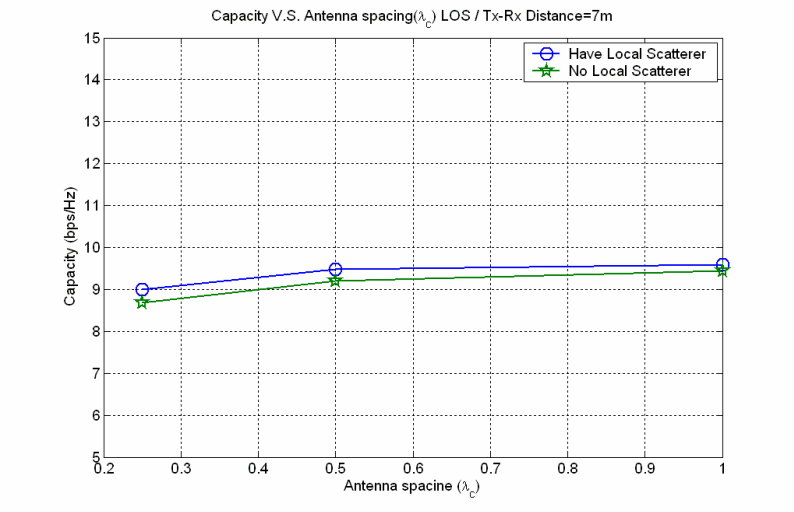

(a)

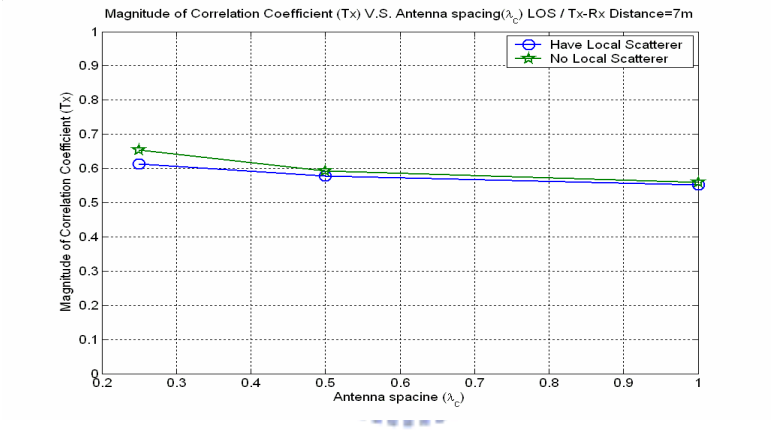

(b)

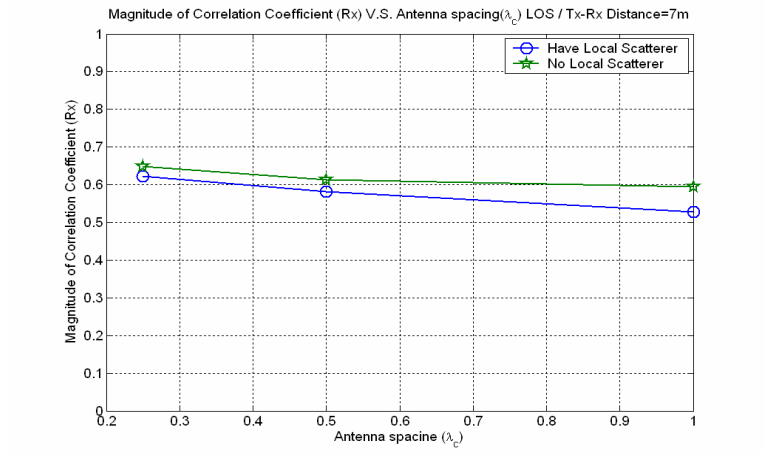

(c)

Fig. 4-6 Local Scatterers discussion under LOS condition in site D (scenarios I/II)

(a) Capacity (b) ρ_{Tx} (c) ρ_{Rx} versus antenna spacing at Tx-Rx Distance=7m

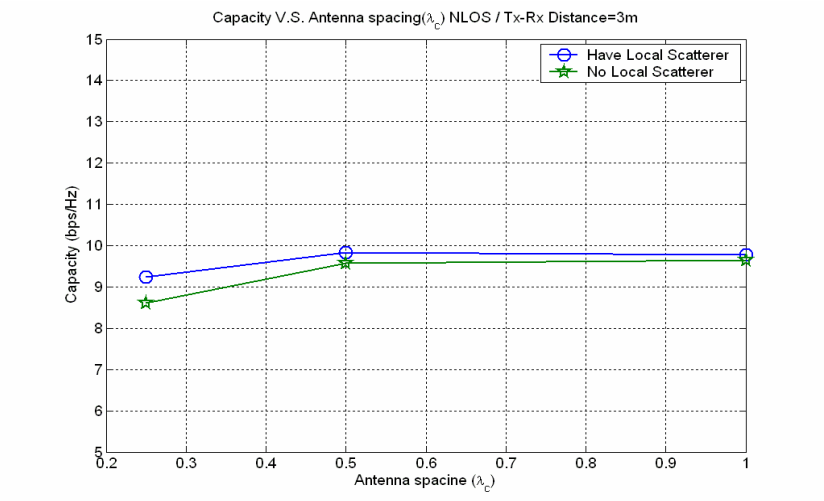

(a)

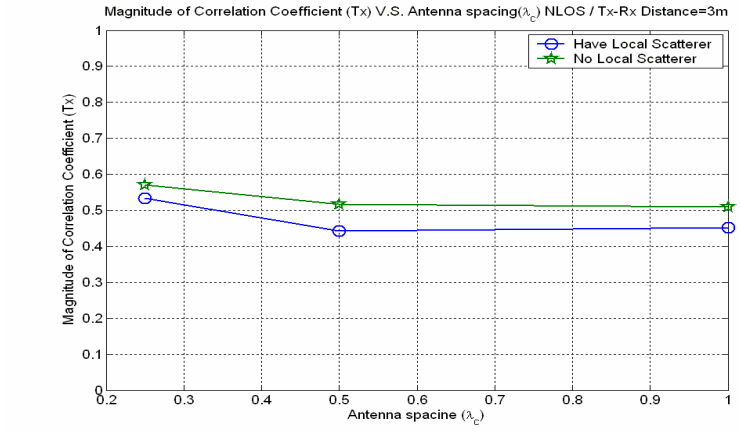

(b)

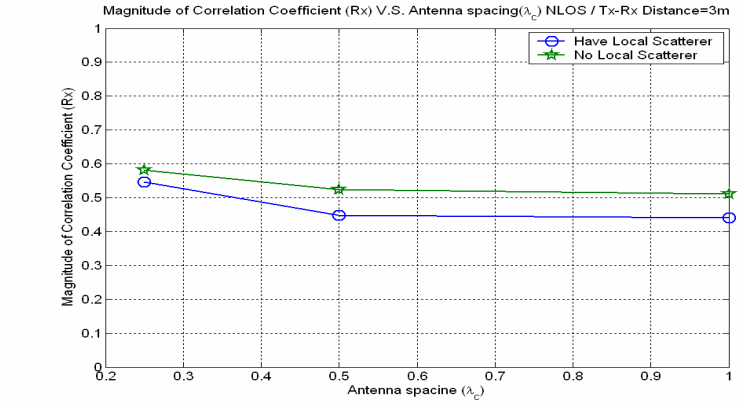

(c)

Fig. 4-7 Local Scatterers discussion under NLOS condition in site D (scenarios III/IV)

(a) Capacity (b) ρ_{Tx} (c) ρ_{Rx} versus antenna spacing at Tx-Rx Distance=3m

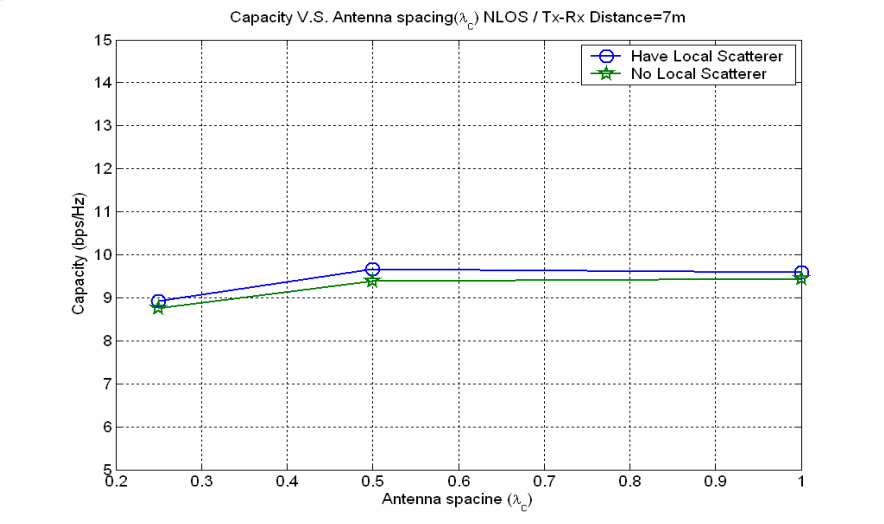

(a)

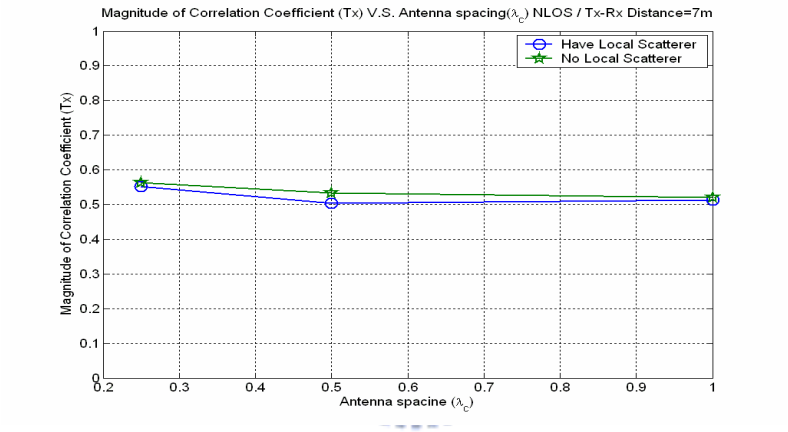

(b)

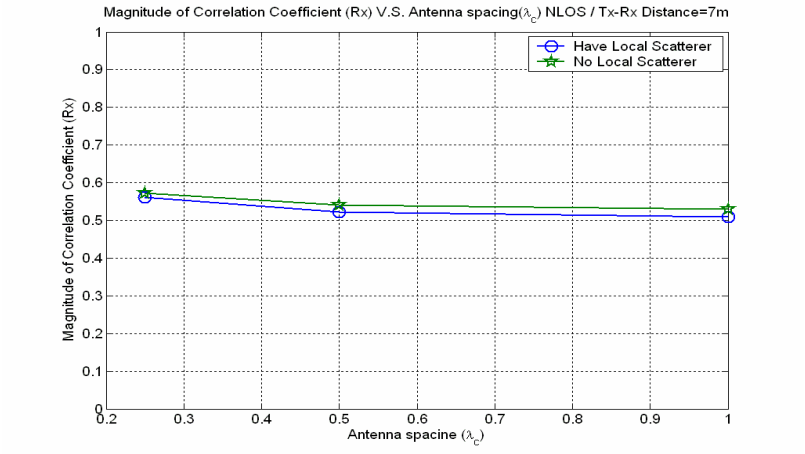

(c)

Fig. 4-8 Local Scatterers discussion under NLOS condition in site D (scenarios III/IV)

(a) Capacity (b) ρ_{Tx} (c) ρ_{Rx} versus antenna spacing at Tx-Rx Distance=7m

4.4 Antenna Spacing Effect (Scenarios I/II/III/IV)

In the UWB-MIMO system, channel capacity may be improved by adaptively changing the element spacing. Changing the element spacing is a way to provide spatial diversity to a MIMO link without increasing the number of antenna array elements [17]. In this section, we adjust the element spacing of virtual antenna arrays to investigate how the capacity varies is with small changes in element locations. During the measurement, the measurement points from P1 to P6 have been selected to consider scenarios I/II/III/IV. And the antenna broadside direction is perpendicular to the direct path direction.

Fig. 4-9(a) (b) (c) illustrates the capacity, Tx and Rx correlation coefficients versus antenna spacing for LOS condition respectively (scenarios I/II). For comparison, the capacity for a perfect Rayleigh channel is plotted. To this end, 10^6 random matrices with independent, identically distributed complex numbers (normal distribution with zero mean and variance $\sigma = 1$) were generated and the averaged capacity was calculated. In the LOS condition, the capacity is low to 6.5 bps/Hz at 0.1λ spacing and dramatically rises to about 10 bps/Hz at 0.5λ spacing. Afterward, capacity grows slowly with the antenna spacing increasing. Both ρ_{Tx} and ρ_{Rx} decrease with antenna spacing increasing.

Fig. 4-10(a) (b) (c) illustrates the capacity, Tx and Rx correlation coefficients versus antenna spacing for NLOS condition respectively (scenarios III/IV). In the NLOS condition, the capacity is low to about 7 bps/Hz at 0.1λ spacing and rise to about 10.5 bps/Hz at 0.5λ spacing. The capacity is not changed while antenna spacing is larger than 1λ.

From the result of this section, we can see that antenna spacing may affect UWB-MIMO capacity significantly under any environment (scenarios I/II/III/IV). And we can find that the capacity increases as the element spacing increases and it saturates when the spacing is larger than 0.5λ. This reveals that the correlation distance between the elements in indoor environments is about 0.5λ.

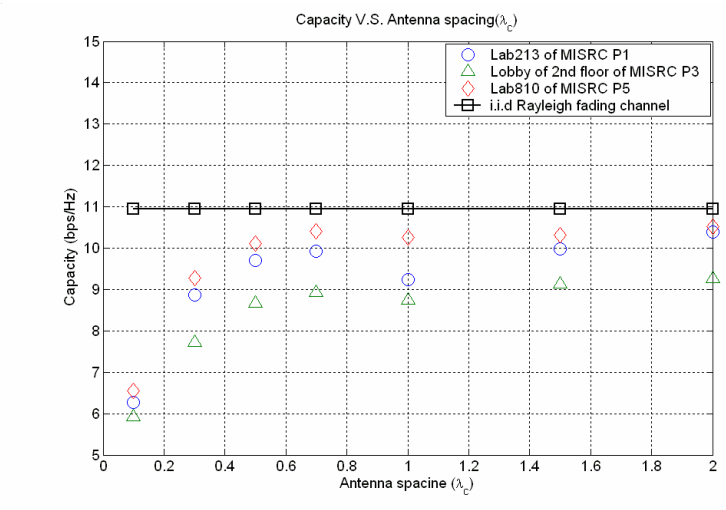

(a)

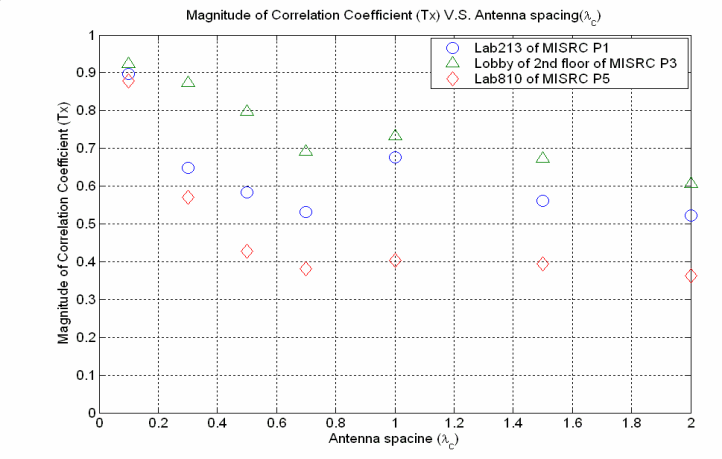

(b)

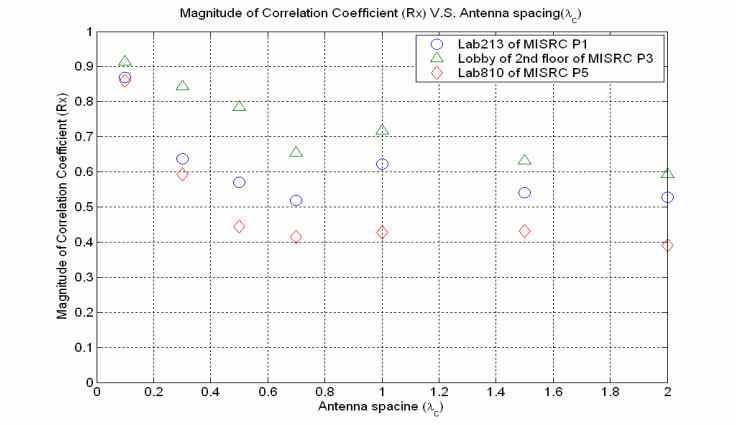

(c)

Fig. 4-9 (a) Capacity (b) ρ_{Tx} (c) ρ_{Rx} versus antenna spacing in LOS condition (P3 belong to the scenario I and P1、P5 belong to the scenario II)

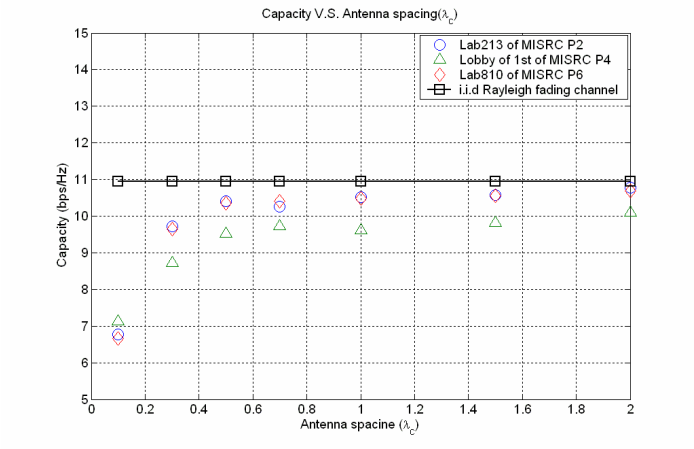

(a)

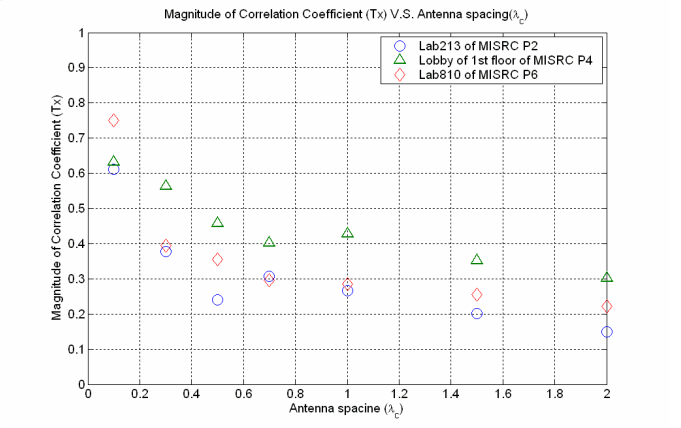

(b)

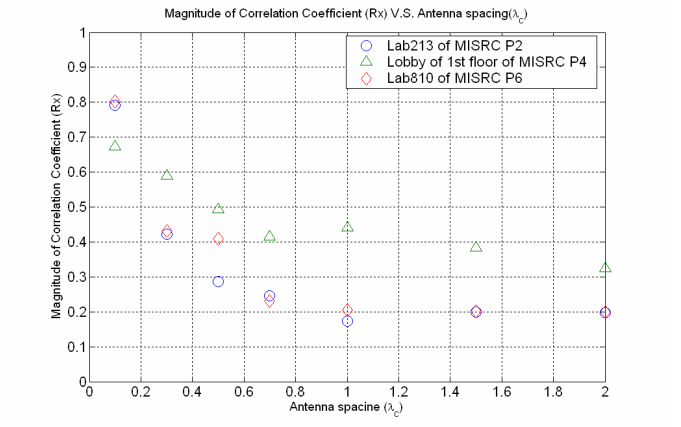

(c)

Fig. 4-10 (a) Capacity (b) ρ_{Tx} (c) ρ_{Rx} versus antenna spacing in NLOS condition (P4 belong to the scenario III and P2, P6 belong to the scenario IV)

4.5 Array Orientation Effect

To investigate the array orientation effect on capacity and correlation, we perform the measurement for a (5×5) UWB-MIMO system in two kinds of indoor environments: one is in a corridor(site E, scenarios V/VI), another one is in a laboratory(site F, scenarios II/IV). During the measurement, two kinds of array orientation are considered: the antenna array broadside orientation direction is perpendicular (orientation I) and parallel (orientation II) to the direct-path direction [4] [18].

4.5.1 Measured results in the scenarios V and VI (corridor, site E)

In Fig. 4-11 and 4-12 (site E), the mean capacities for different array size ($n_T = n_R$) is shown. From Fig. 4-11, we observe a significant different between the capacities achieved by parallel and perpendicular arrays in all distance. The perpendicular array results in a higher capacity gain than the parallel array in LOS condition (scenario V). This is because the perpendicular receiver array allows additional spatial dimensions of the UWB-MIMO channel by distinguishing between those scatterers on the opposite walls of the corridor with the same distance to the receiver array. The parallel array would be unable to distinguish between these ‘mirrored’ scatterers and hence capacity gain for orientation II is significantly lower. Fig. 4-13 shows the correlation coefficients for scenario V. As expected, the receiver correlation is higher when the broadside of the receive array is parallel to LOS in all distance because perpendicular array will distinguish more multipath, so can reduce the correlation coefficient. The transmit correlations are almost equal for two orientations.

The above effect is that we measured for LOS condition in the corridor (scenario V). And now let us observe that in case of NLOS condition (scenario VI), whether the characteristic we measure is the same as LOS condition? Fig. 4-12 is the result of measured in the scenario VI. From fig.4-12, we find that orientation I results in a higher capacity gain

than orientation II. The reason is the same as above result. Fig. 4-14 shows the correlation coefficient for the scenario VI.

In addition, we also observe the capacity increases linearly with the number of antenna elements, indicating that there are a sufficient number of strong MPCs providing independent transmission paths for different data streams.

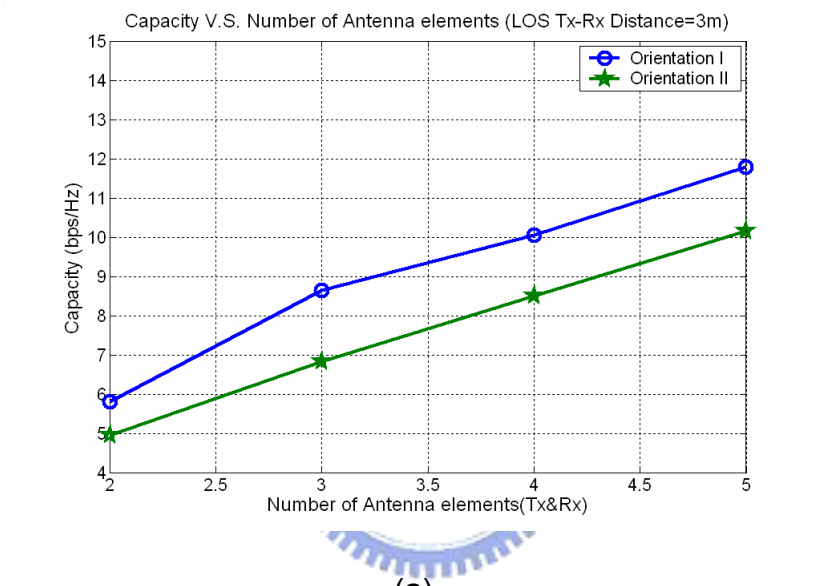

(a)

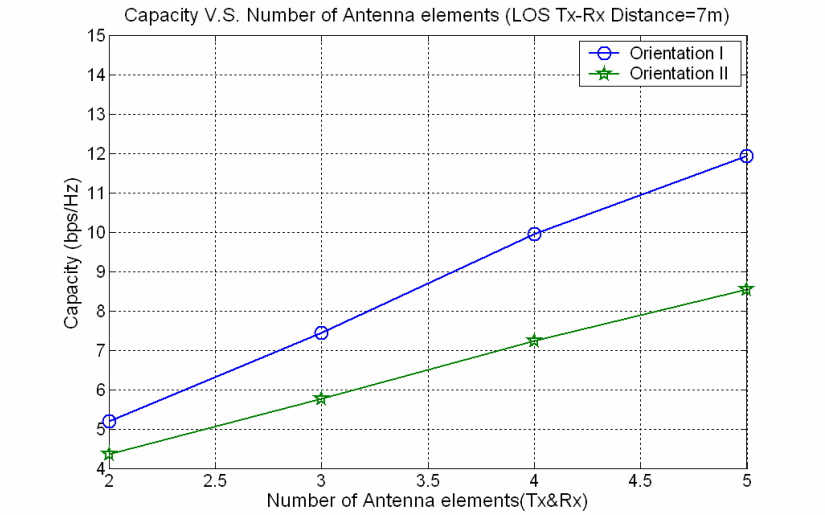

(b)

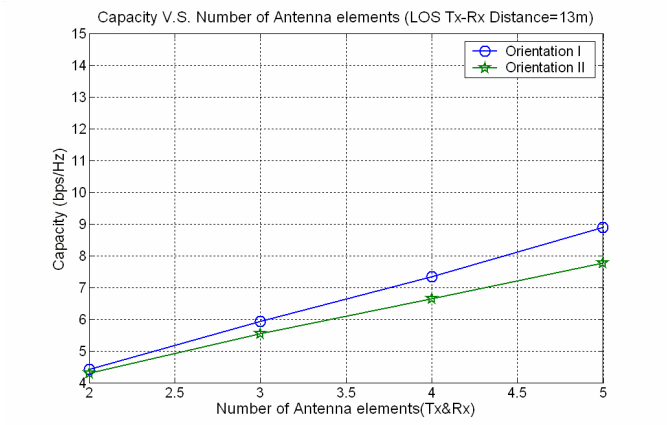

(c)

Figure 4-11 Capacity versus array orientations in the scenario V (site E, LOS)

(a) Tx-Rx Distance=3m (b) Tx-Rx Distance=7m (c) Tx-Rx Distance=13m

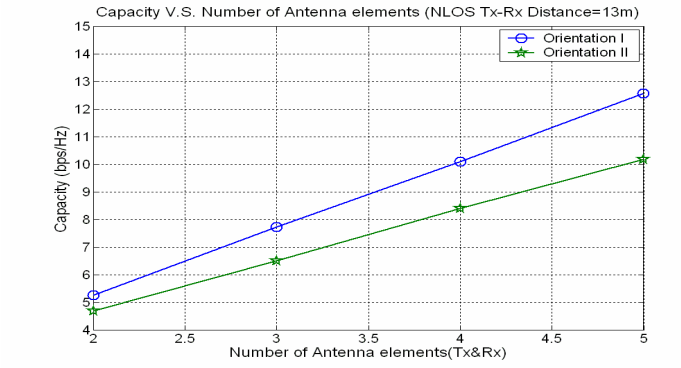

(a)

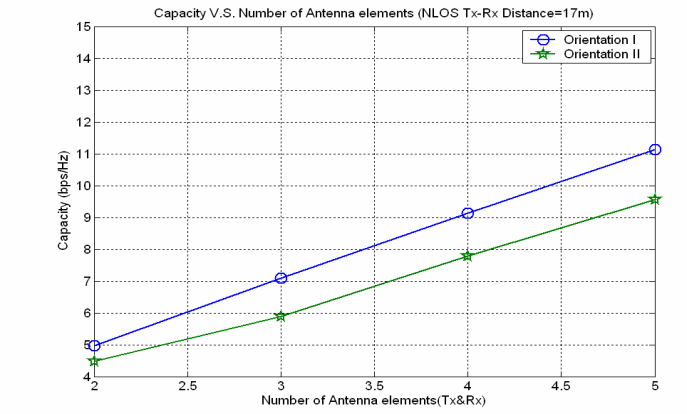

(b)

Figure 4-12 Capacity versus array orientations in the scenario VI (site E, NLOS)

(a) Tx-Rx Distance=13m (b) Tx-Rx Distance=17m

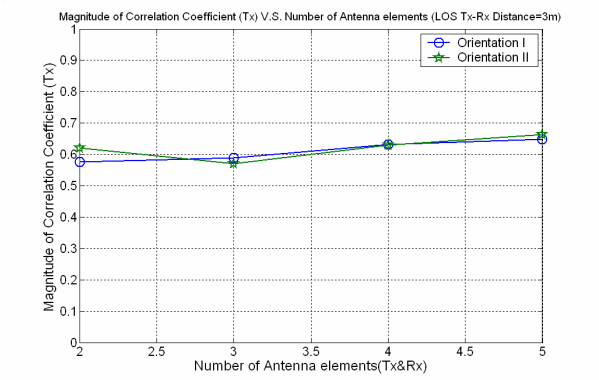

(a)

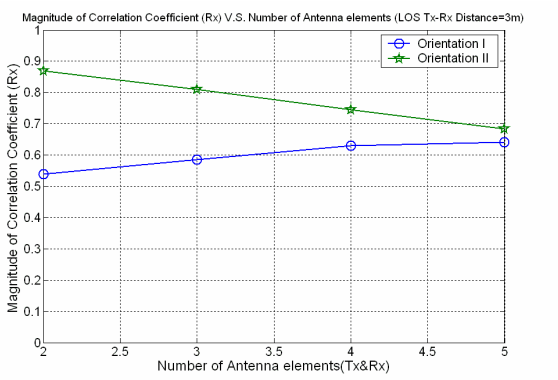

(d)

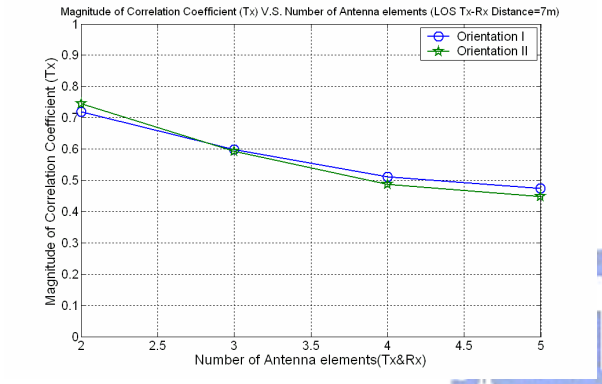

(b)

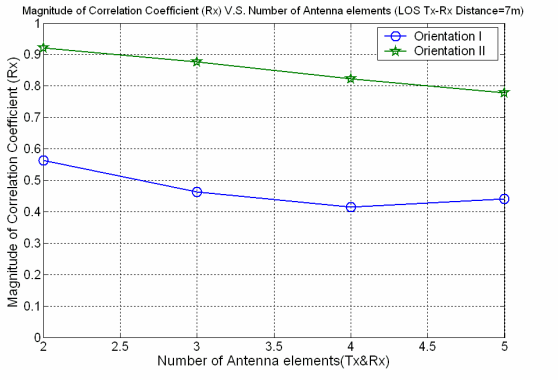

(e)

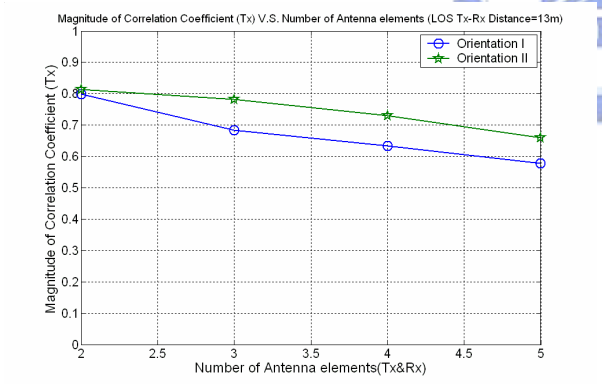

(c)

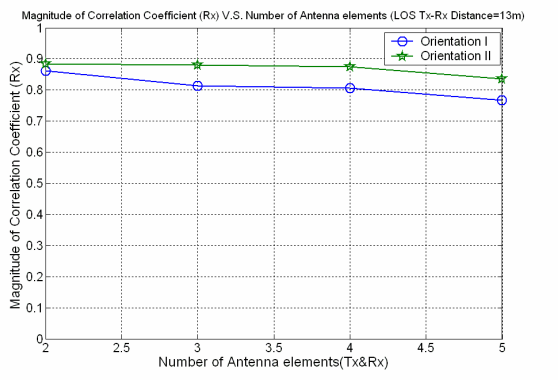

(f)

Fig 4-13 ρ_{Tx} and ρ_{Rx} versus array orientations in the scenario V (site E, LOS)

(a) ρ_{Tx} Tx-Rx Distance=3m (d) ρ_{Rx} Tx-Rx Distance=3m

(b) ρ_{Tx} Tx-Rx Distance=7m (e) ρ_{Rx} Tx-Rx Distance=7m

(c) ρ_{Tx} Tx-Rx Distance=13m (f) ρ_{Rx} Tx-Rx Distance=13m

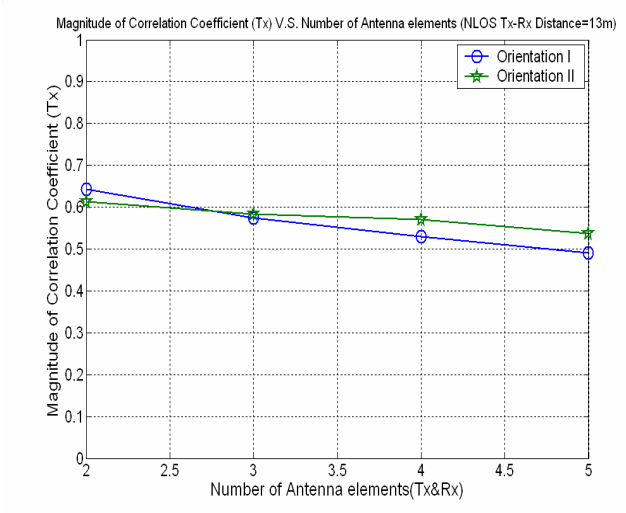

(a)

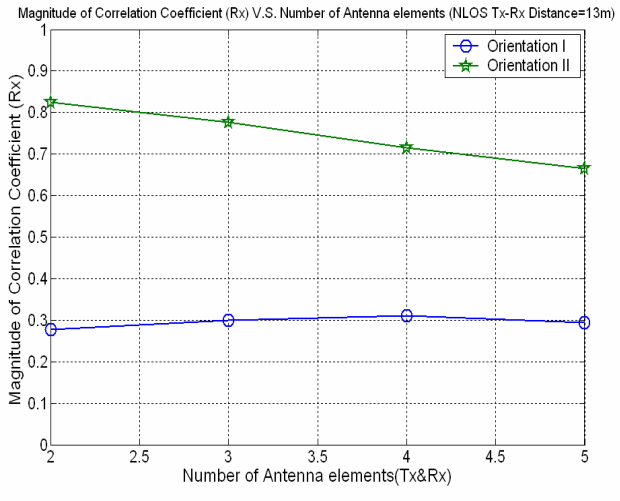

(c)

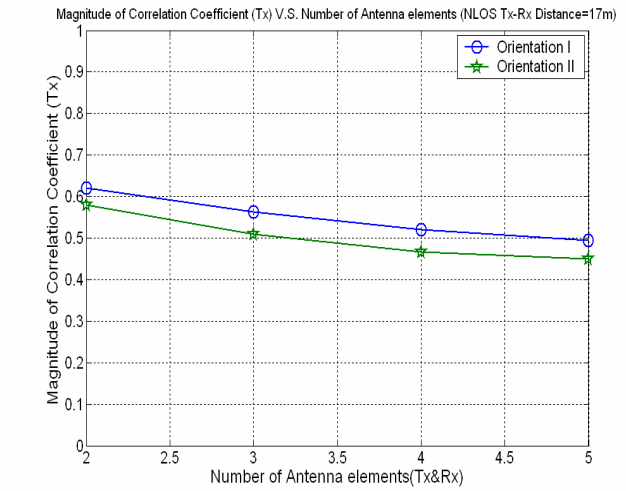

(b)

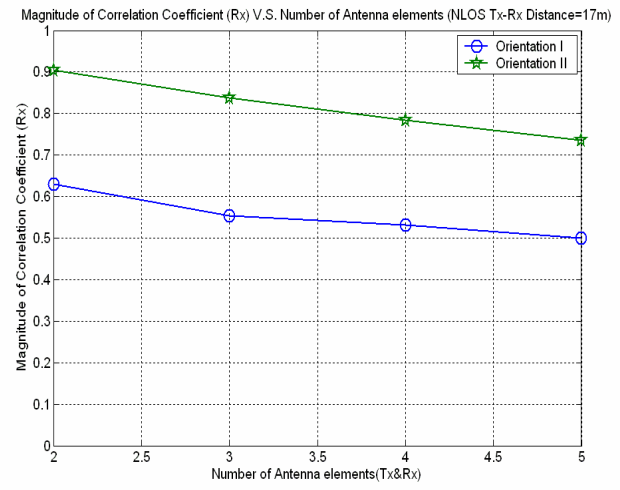

(d)

Fig 4-14 ρ_{Tx} and ρ_{Rx} versus array orientations in the scenario VI (site E, NLOS)

(a) ρ_{Tx} Tx-Rx Distance=13m (c) ρ_{Rx} Tx-Rx Distance=13m

(b) ρ_{Tx} Tx-Rx Distance=17m (d) ρ_{Rx} Tx-Rx Distance=17m

4.5.2 Measured results in the scenarios II and IV (laboratory, site F)

Above-mentioned is the measured result in the corridor (scenarios V/VI), and then we observe the result in the laboratory (scenarios II/IV) below. Fig. 4-15 and 4-16 illustrate the capacity for both LOS and NLOS conditions in the laboratory (scenarios II and IV). From Fig. 4-15, in the far distance between Tx, Rx the capacity for orientation I is more than orientation II, but when the near distance between Tx, Rx, it is similar for both orientation. The reason for this phenomenon is that when the distance between Tx, Rx is far, the correlation coefficient will be drop. Therefore, when receiver array broadside parallel to the direct path will cause correlation coefficient increased, then capacity will be drop. But when the distance between Tx, Rx is near, the path of LOS is stronger than others. So both two orientations have high correlation coefficient, and then capacity is low equally. Fig. 4-17 shows the correlation coefficient in the scenario II.

From Fig.4-16 we can see that in the NLOS condition, the capacity is similar for both orientations in all distance between Tx and Rx. This is because no dominant path exists under NLOS scenarios where no additional spatial diversity can be obtained by changing the orientations. Fig. 4-18 shows the correlation coefficient in the scenario IV.

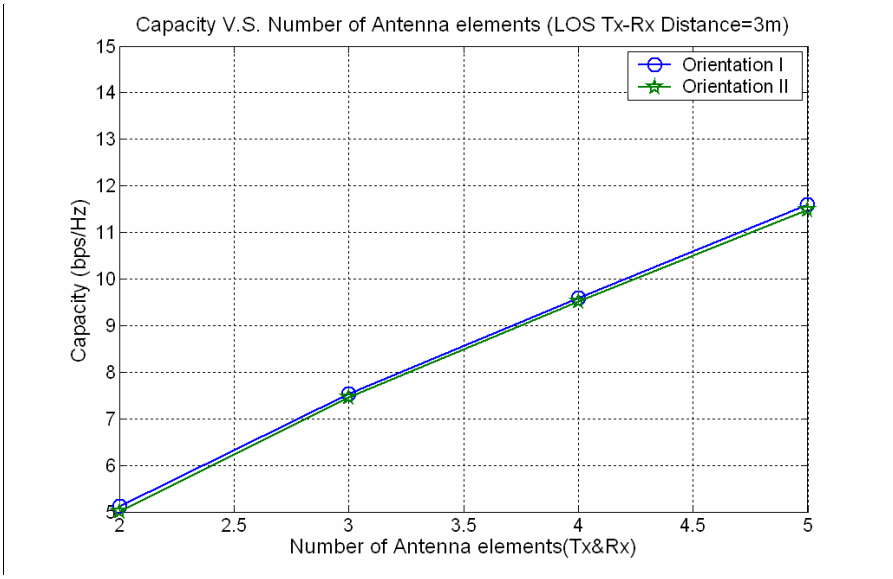

(a)

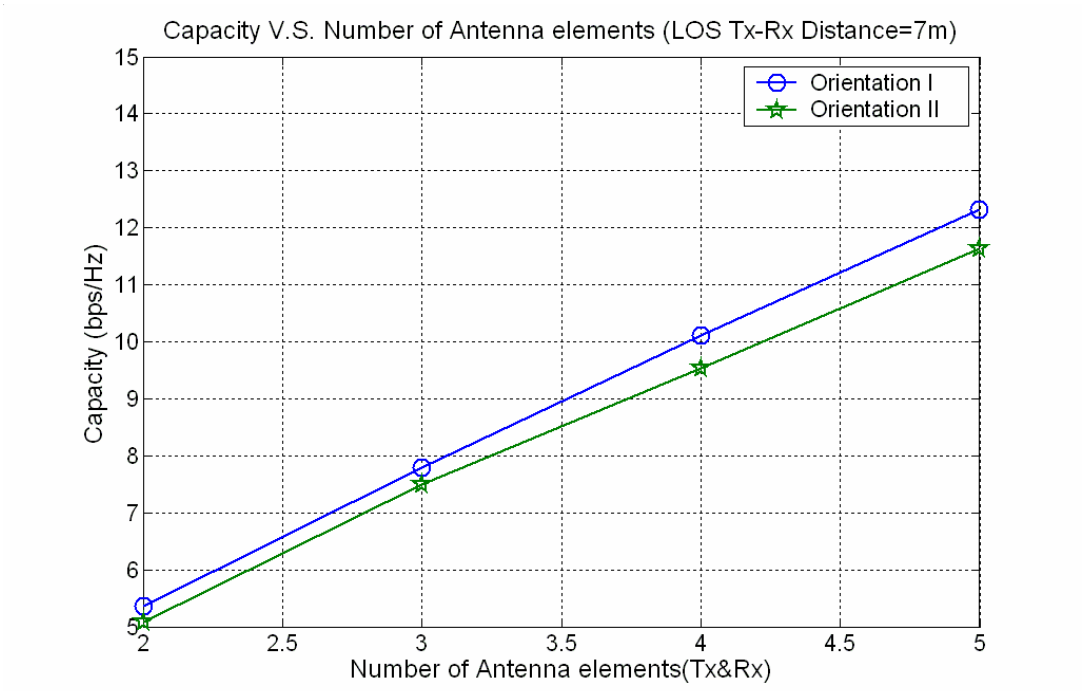

(b)

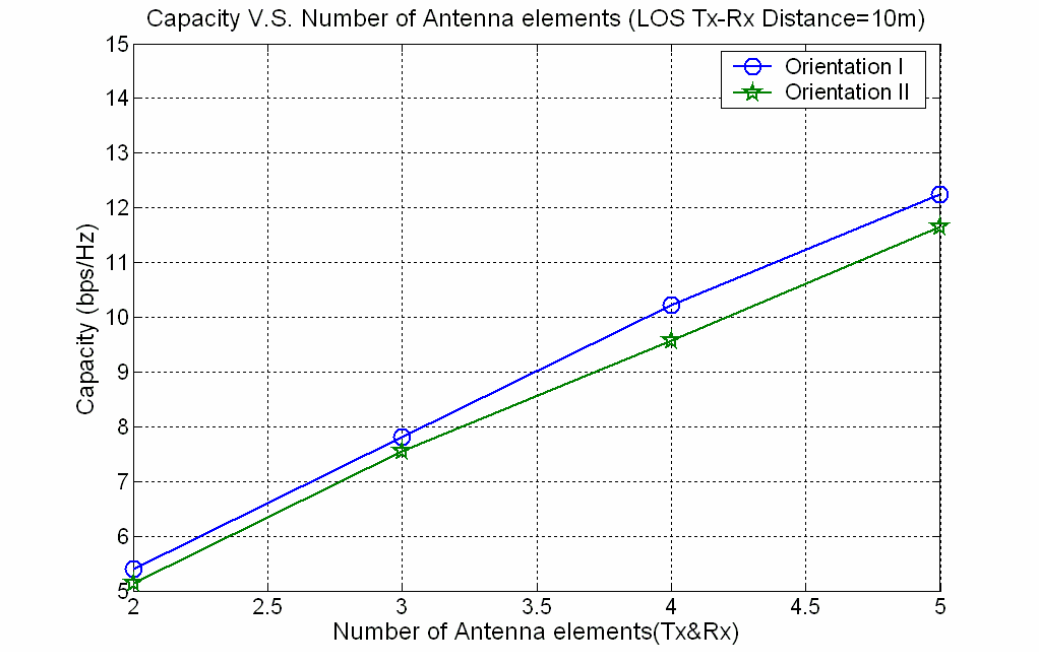

(c)

Figure 4-15 Capacity versus array orientations in the scenario II (site F, LOS)

(a) Tx-Rx Distance=3m (b) Tx-Rx Distance=7m (c) Tx-Rx Distance=10m

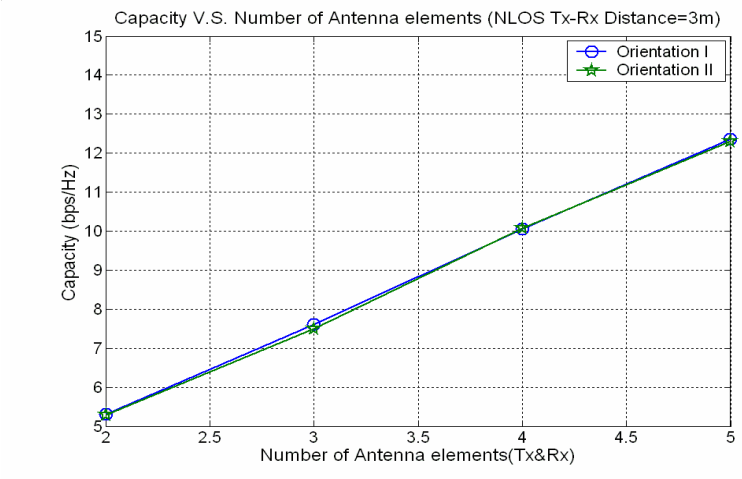

(a)

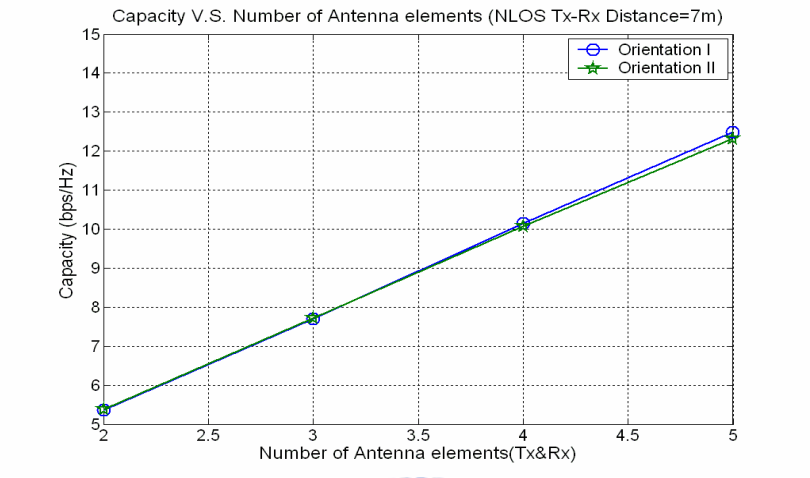

(b)

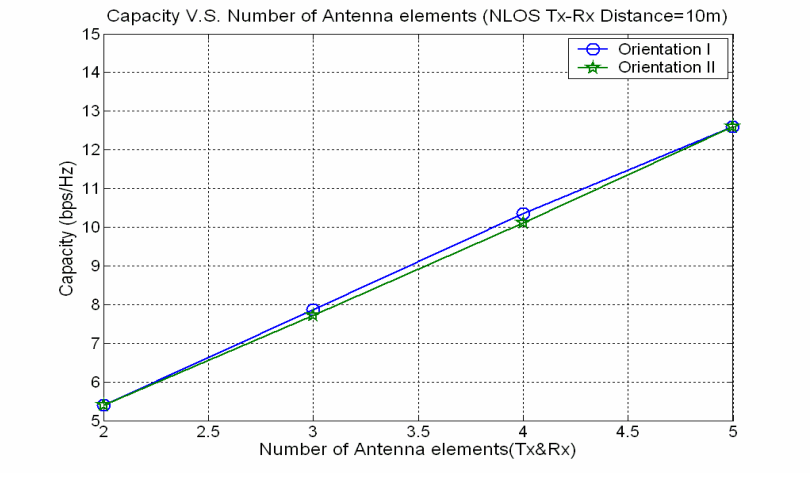

(c)

Figure 4-16 Capacity versus array orientations in the scenario IV (site F, NLOS)

(a) Tx-Rx Distance=3m (b) Tx-Rx Distance=7m (c) Tx-Rx Distance=10m

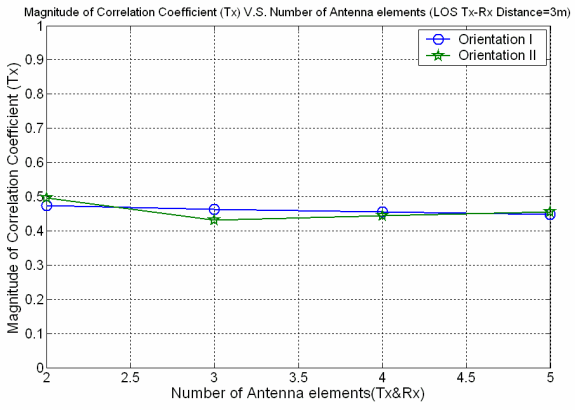

(a)

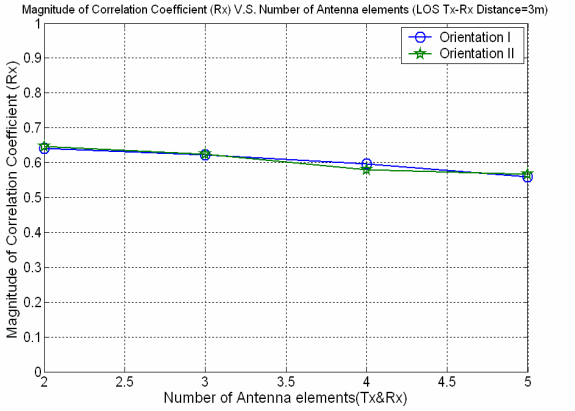

(d)

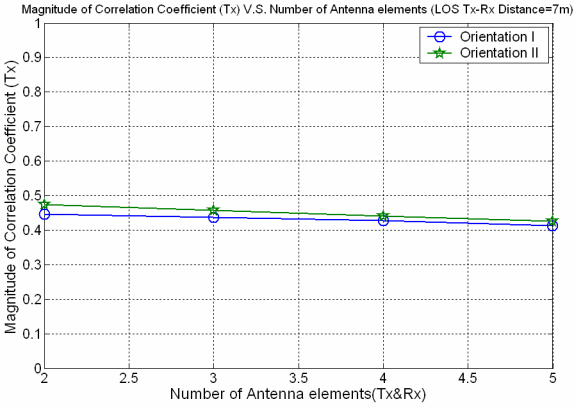

(b)

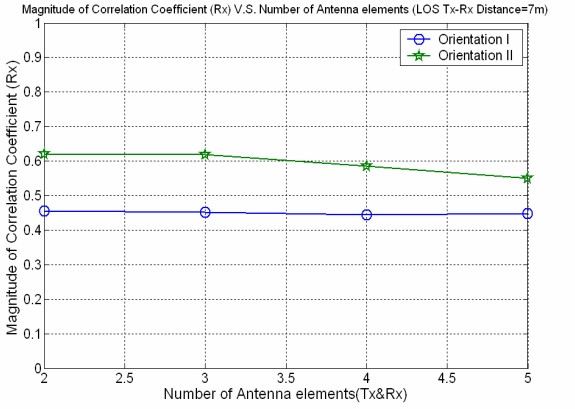

(e)

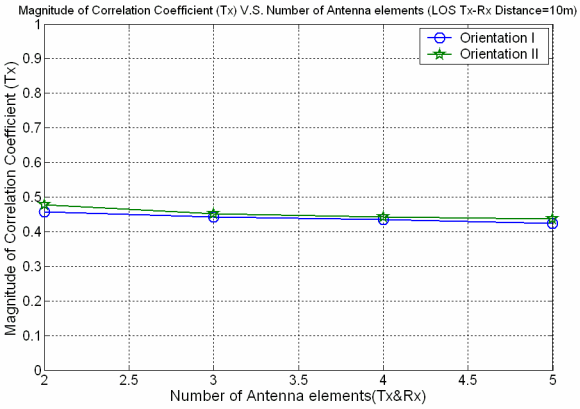

(c)

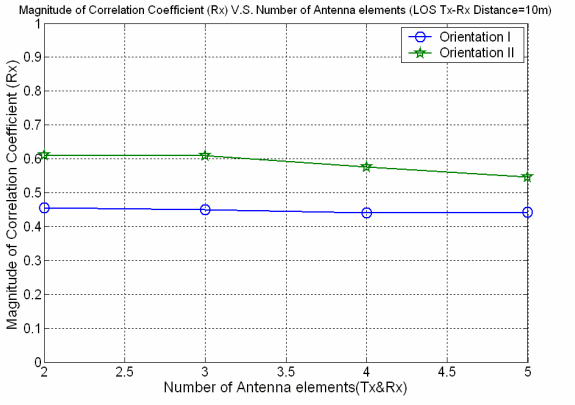

(f)

Fig 4-17 ρ_{Tx} and ρ_{Rx} versus array orientations in the scenario II (site F, LOS)

(a) ρ_{Tx} Tx-Rx Distance=3m (d) ρ_{Rx} Tx-Rx Distance=3m

(b) ρ_{Tx} Tx-Rx Distance=7m (e) ρ_{Rx} Tx-Rx Distance=7m

(c) ρ_{Tx} Tx-Rx Distance=10m (f) ρ_{Rx} Tx-Rx Distance=10m

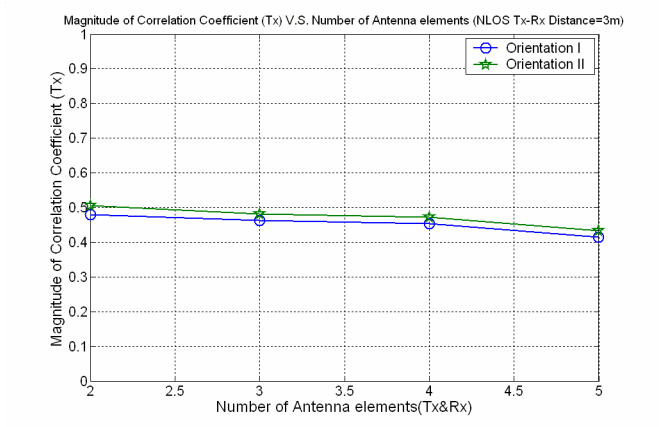

(a)

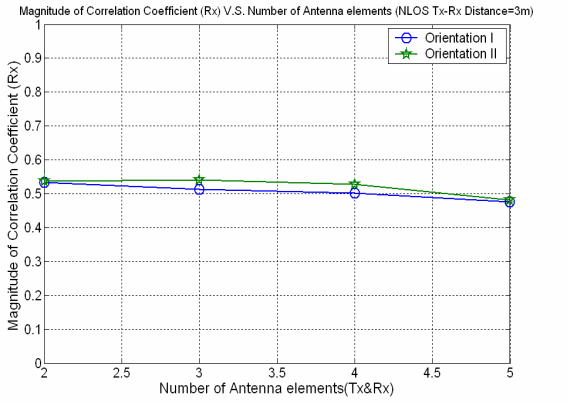

(d)

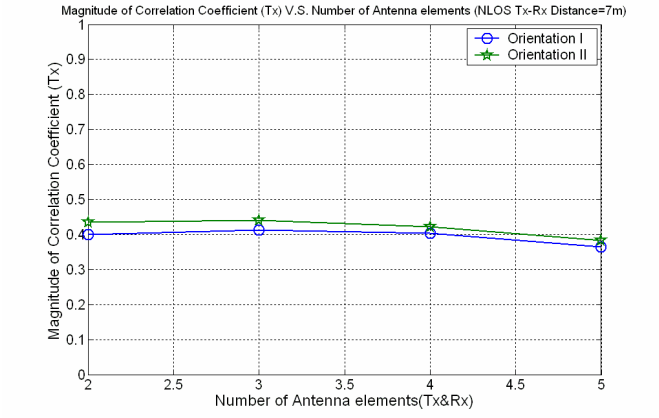

(b)

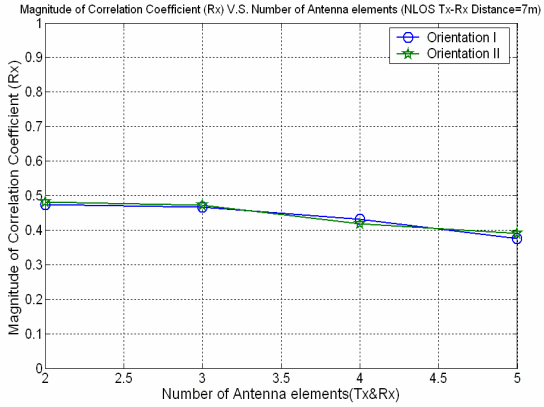

(e)

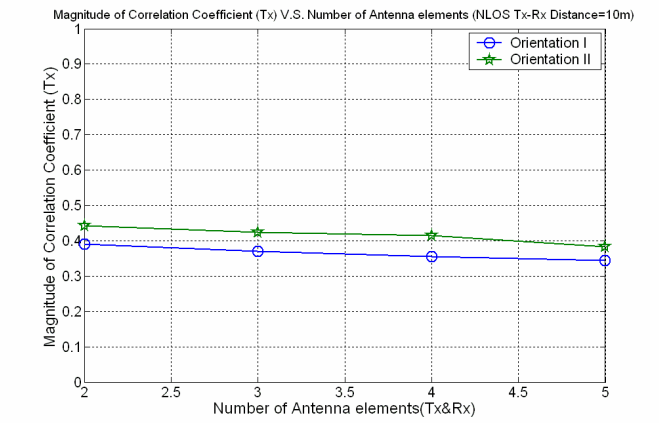

(c)

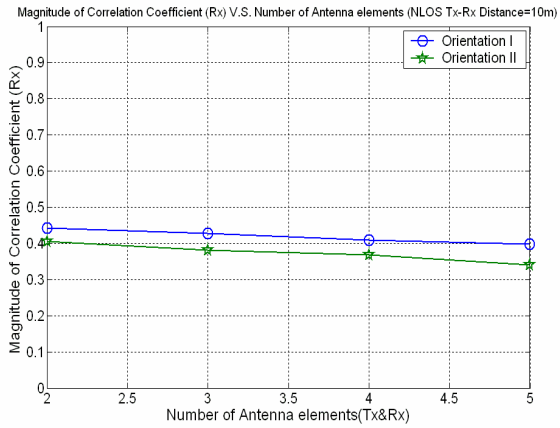

(f)

Fig 4-18 ρ_{Tx} and ρ_{Rx} versus array orientations in the scenario IV (site F, NLOS)

(a) ρ_{Tx} Tx-Rx Distance=3m (d) ρ_{Rx} Tx-Rx Distance=3m

(b) ρ_{Tx} Tx-Rx Distance=7m (e) ρ_{Rx} Tx-Rx Distance=7m

(c) ρ_{Tx} Tx-Rx Distance=10m (f) ρ_{Rx} Tx-Rx Distance=10m

4.6 Capacity Loss

In this section, for a more in-depth analysis of the performance of UWB-MIMO systems at locations with high SNR and high antenna correlation, measurements were done to investigate the effects of SNR and antenna correlation on UWB-MIMO channel capacity. First of all, we define capacity loss (C_{loss}) as

$$C_{loss} = 1 - \frac{C_{measure}(SNR)}{C_{i.i.d}(SNR)} \tag{4-1}$$

The capacity loss for different measurement is calculated for comparing the measured capacity and the optimum case at the same SNR.

4.6.1 Capacity Loss for different antenna spacing

The measurement points from P1, P2 have been selected to consider LOS and NLOS condition. The channel capacity loss with respect to the received SNR for various antenna spacing are calculated from Eq.4-1 and shown in Fig.4-19. From Fig.4-19, we can see that for small antenna spacing, when SNR increases, the channel capacity loss increases initially but decreases gradually afterwards. The reason for this is that when SNR is low, a comparison of the ideal channel and the measured channel shows that there is a channel capacity gap which widens as SNR increases. However, when SNR increases beyond a certain value, this gap becomes constant and independent of the SNR. It means that the relative channel capacity loss due to the effect of high antenna correlation is reduced as SNR increases. In other words, Fig.4-19 shows that in small antenna spacing, the UWB-MIMO system is robust against the high antenna correlation when SNR is high.

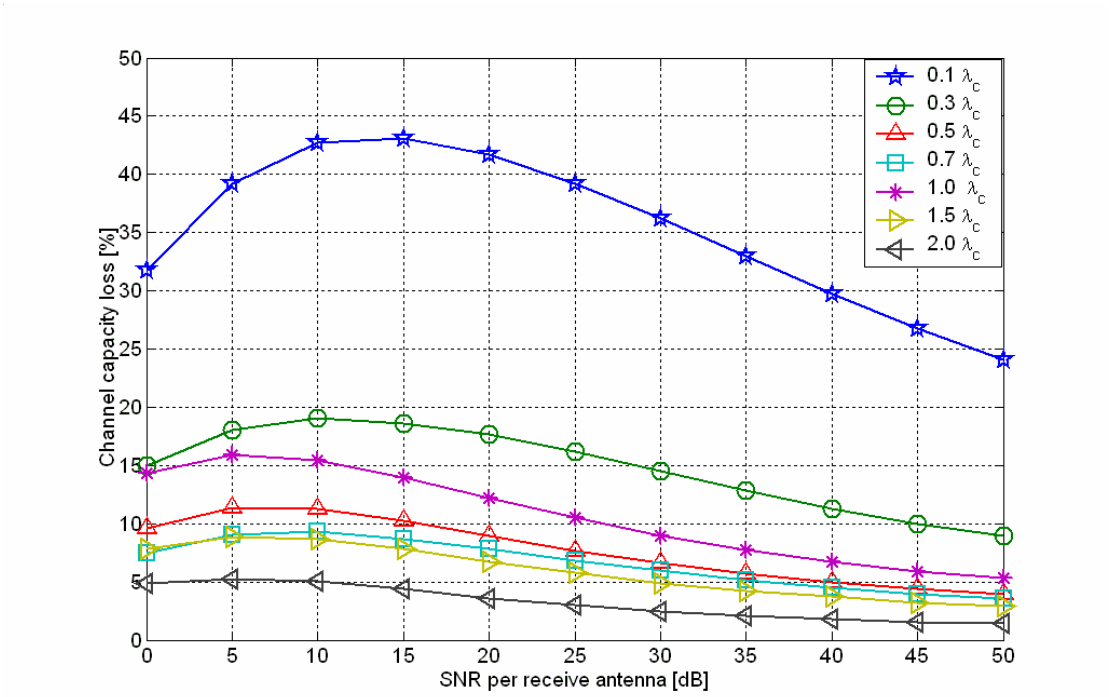

(a)

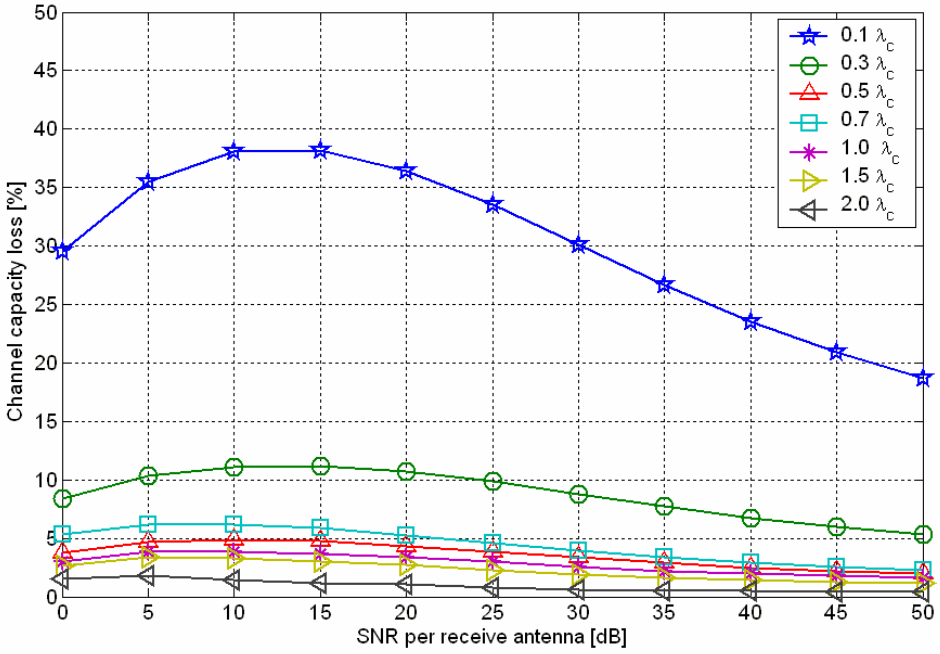

(b)

Fig. 4-19 Capacity loss versus SNR at different antenna spacing

(a) measured point P1 in LOS condition

(b) measured point P2 in NLOS condition

4.6.2 Capacity loss for different Tx-Rx distance in LOS condition

From section 4-2, we know that when Tx-Rx distance is in near distance, channel capacity is low and antenna correlation is high in the LOS condition. However from the propagation point of view, the dominant LOS signal component would also lead to a high receive signal power which increases channel capacity when Tx-Rx distance is in near distance. It becomes a situation where there is a tradeoff between the effects of increased correlation and increased receive SNR on the UWB-MIMO channel capacity. Therefore we make a further analysis in the site B and site C.

Fig.4-20 illustrates the capacity loss versus SNR at different Tx-Rx distance in the scenarios I and II. From Fig.4-20 (a), we can see that for small Tx-Rx distance, when SNR increases, the channel capacity loss increases initially but decreases gradually afterwards. The reason is same as section 4.6.1. But when Tx-Rx distance is added to 10m, the capacity loss is almost same at different SNR. This phenomenon tell us that when Tx-Rx distance is in near distance, although antenna correlation is high but if received SNR is excess 10dB then the UWB-MIMO system is robust against the antenna correlation.

Above results are measured in the scenario I, now we observe the measured result in the scenario II. The main difference of scenarios I and II is that there are heavy clutter in the scenario II. From Fig.4-20 (b), we can see that when Tx-Rx distance is in near distance, the capacity loss is not as high as measured results in the scenario II. This is because there are scatterers in the scenario II, so antenna correlation is not as high as the scenario I. So if antenna correlation is not high, capacity loss will not change when SNR increases.

From above results, we find that the loss of channel capacity owing to high correlation is significantly reduced when the SNR is sufficiently high.

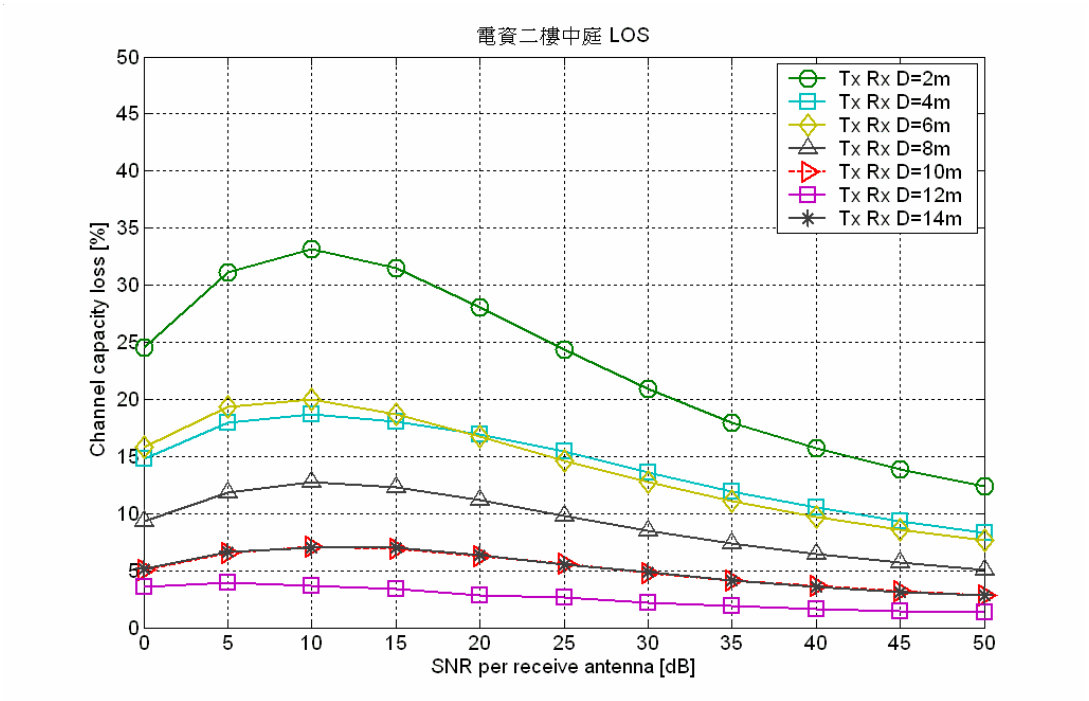

(a)

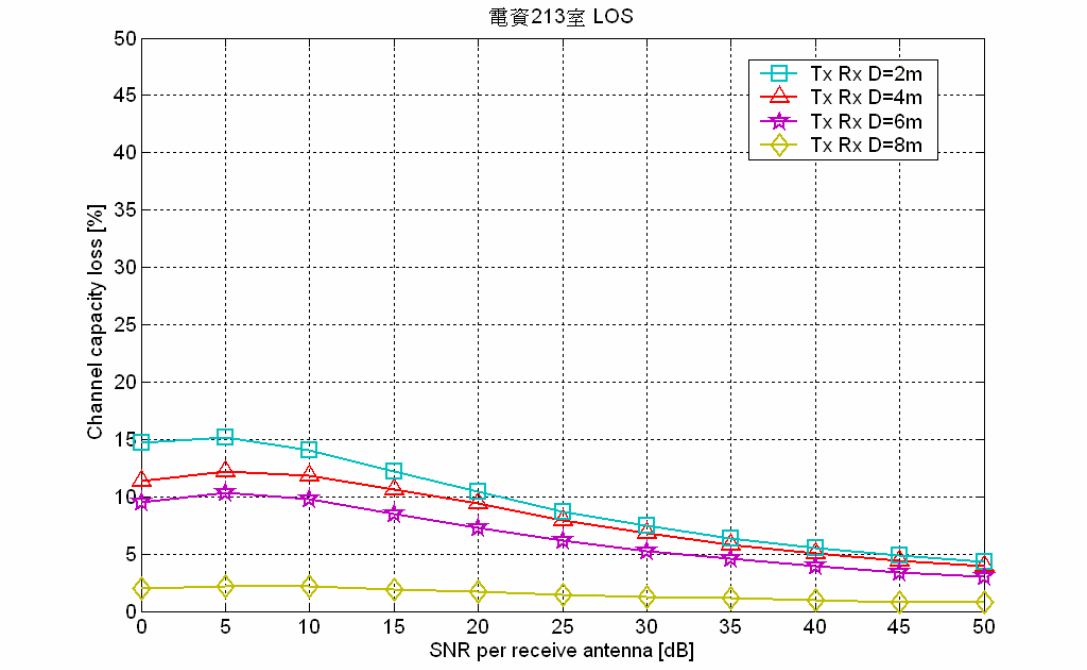

(b)

Fig. 4-20 Capacity loss versus SNR at different Tx-Rx distance in LOS condition

(a) measured path1 in the scenario I (site B)

(b) measured path3 in the scenario II (site C)

4.7 Bandwidth Effect

In this section, we investigate the impact of the signal bandwidth on the UWB-MIMO capacity. We choose 20、40、80、500 and 1000M signal bandwidths to see how it affects the capacity. From figures 4-21 we can see that a small difference in capacity when using the larger bandwidth. Hence not much frequency diversity is available.

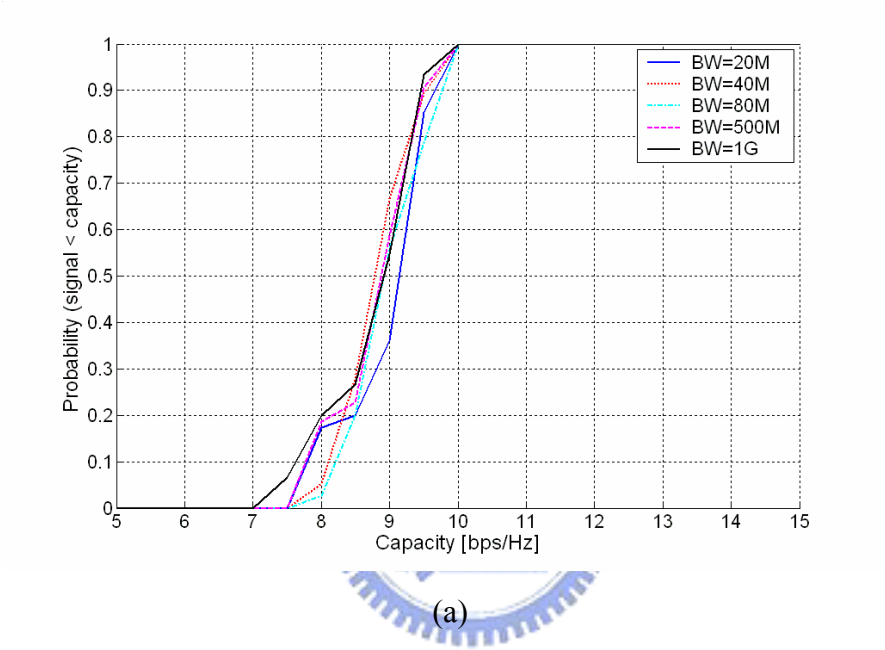

(a)

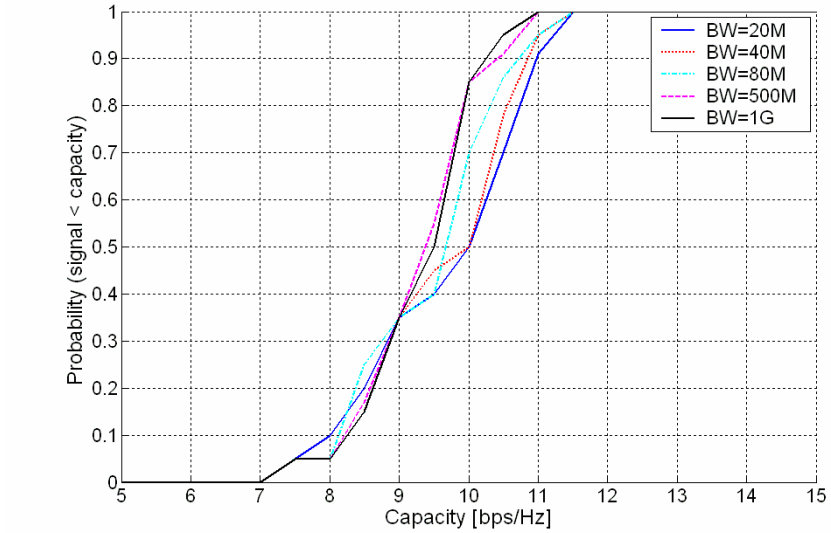

(b)

Fig. 4-21 CDF for capacity (a) LOS (b) NLOS

Chapter 5

Characterization of UWB Channels for indoor environment

This chapter presents the characterization of UWB channels for indoor environment with above measured data. This channel characterization addresses only the small scale propagation properties. The Saleh-Valenzuela (S-V) model [19] is used as a basis for our UWB channel model.

5.1 Radio Channel Model

For the small scale properties, we have chosen the S-V model [19] as a basis for parameter extraction. In the S-V model, multipath components (MPCs) behave like rays arriving in clusters. This results in the following discrete time impulse response for the channel:

$$h(t) = \sum_{l=0}^{L} \sum_{k=0}^{K} \beta_{k,l} \delta(t - T_l - \tau_{k,l}) \qquad (5\text{-}1)$$

where $\beta_{k,l}$ is the tap weight of the kth component in the lth cluster, T_l represents the arrival time of the lth cluster, and $\tau_{k,l}$ is the arrival time of the kth arrival within the lth cluster, relative to T_l. K is the total number of MPCs in a cluster and L is the total number of clusters. By definition, $\tau_{o,l} = 0$.

The distributions of the cluster and ray arrival times, i.e. T_l and $\tau_{k,l}$, are given by Poisson processes in the following equations:

$$p\left(T_l \middle| T_{l-1}\right) = \Lambda \exp\left[-\Lambda\left(T_l - T_{l-1}\right)\right], \quad l > 0$$
$$p\left(\tau_{k,l} \middle| \tau_{(k-1),l}\right) = \lambda \exp\left[-\lambda\left(\tau_{k,l} - \tau_{(k-1),l}\right)\right], \quad k > 0 \tag{5-2}$$

where Λ is the cluster arrival rate and λ is the ray arrival rate.

β_{kl} is a Rayleigh-distributed random variable with a mean-square value that obeys a double exponential decay law, according to

$$\overline{\beta^2}_{kl} = \overline{\beta^2(0,0)}\ \exp\left(-T_l/\Gamma\right)\exp\left(-\tau_{kl}/\lambda\right), \tag{5-3}$$

where $\overline{\beta^2(0,0)}$ is the average power of the first arrival of the first cluster. This average power is a function of the distance separating the transmitter and receiver. Fig. 5-1 illustrates this, showing the mean envelope of a three-cluster channel.

Hence, in order to characterize the multipath statistics of the channel, the parameter Γ, γ, Λ, λ (i.e. cluster and ray power-decay time constants and arrival rates) have to be extracted.

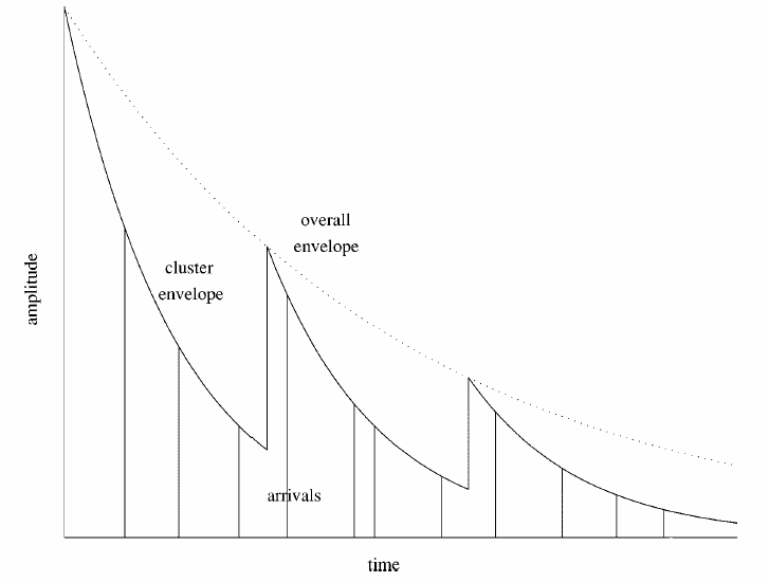

Figure 5-1 An illustration of exponential decay of mean cluster power and ray power within clusters.

5.2 Model Parameters from the Data

The VNA measurements yield the complex frequency responses of the channel. The time domain impulse responses are obtained from these frequency domain data by using simple IFFT. The above procedure yields the PDP for each channel impulse response. The number of clusters and their respective arrival times, w.r.t. T_o are obtained from manual inspection of each PDP.

5.2.1 Cluster and Ray Power-Decay Time Constants, Γ and γ

For the extraction of Γ, the power level of the MPCs in each cluster is divided by $\overline{\beta^2(0,0)}$. Then, all the cluster arrivals, i.e. first MPC in each cluster $\beta_{0,l}$ are superimposed and plotted on a semi-log graph against T_l. Γ is obtained from the plot by applying a least square curve fitting program.

For the extraction of γ, it is assumed in this paper that the MPCs in all clusters decay at a constant rate. The MPCs in each cluster is first normalized w.r.t. the power of the first MPC in that cluster. All the clusters from all PDPs are then superimposed and plotted on a semi-log graph against $\tau_{k,l}$.

5.2.2 Cluster and Ray Arrival Rates, Λ and λ

Cluster and ray arrivals are described by the Poisson process in (5-2). For cluster arrivals, T_0 is set to zero, with all other T_l adjusted accordingly. For ray arrivals, $\tau_{0,l}$ is set to zero, with all other arrival times of rays in the same cluster adjusted accordingly. With these adjustments, the empirical CDF is obtained from the measured data and least mean square (LMS) criteria is used to fit the best exponential CDF (CDF of a Poisson process is an exponential function) to the empirical CDF.

5.3 Measured results in the Scenarios I, II, III, and IV

Fig 5-2, 5-3, 5-4, 5-5 show four parameter of S-V model for scenarios I, II, III and IV.

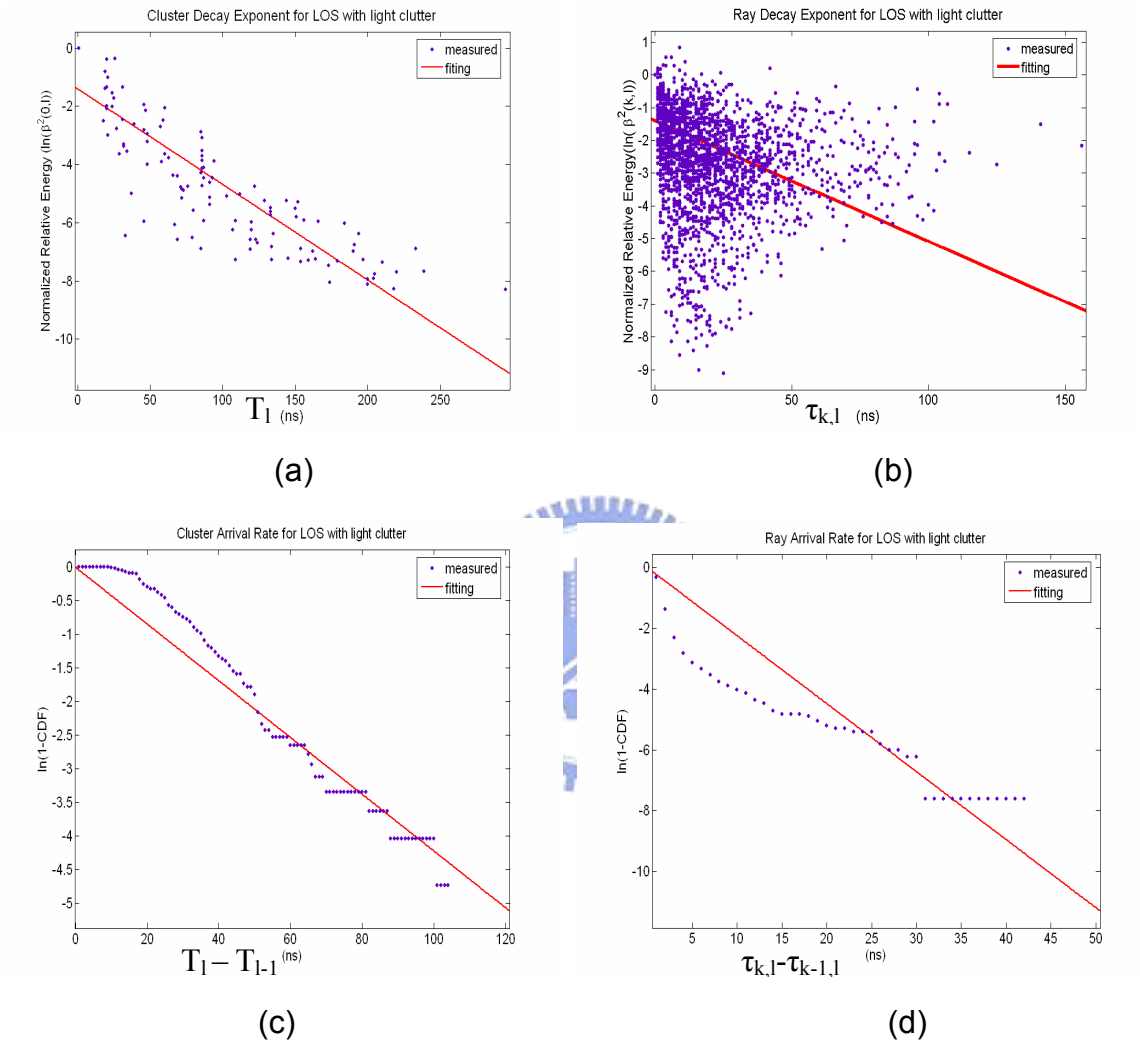

Fig 5-2 Four parameters of S-V model for scenario I

(a) Cluster decay exponent fit for scenario I ($\Gamma = 30.47 \quad ns$)

(b) Ray decay exponent fit for scenario I ($\gamma = 27.12 \quad ns$)

(c) Cluster arrival rate fit for scenario I ($1/\Lambda = 23.7 \quad ns$)

(d) Ray arrival rate fit for scenario I ($1/\lambda = 4.47 \quad ns$)

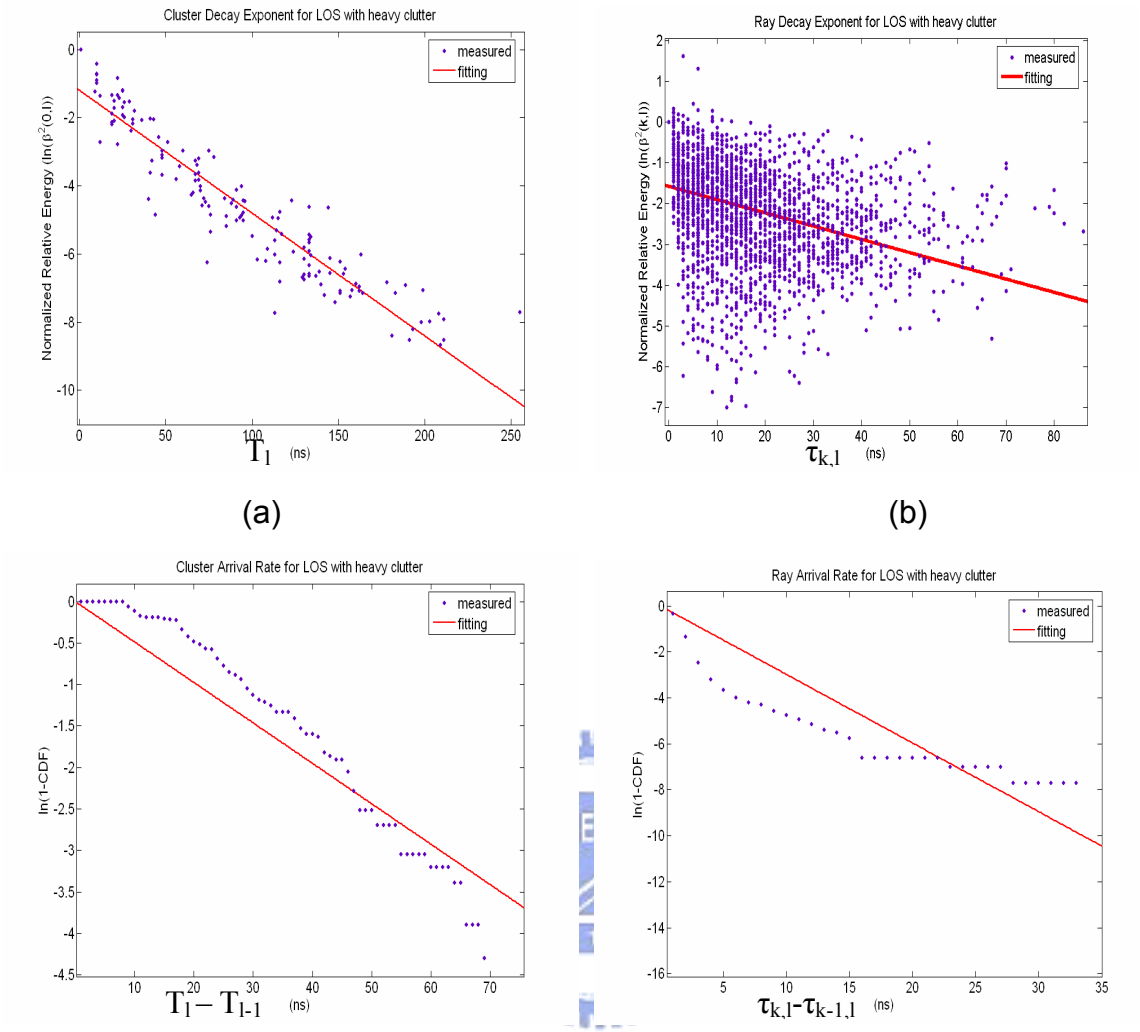

Fig 5-3 Four parameters of S-V model for scenario II

(a) Cluster decay exponent fit for scenario II ($\Gamma = 27.75 \quad ns$)

(b) Ray decay exponent fit for scenario II ($\gamma = 30.77 \quad ns$)

(c) Cluster arrival rate fit for scenario II ($1/\Lambda = 20.51 \quad ns$)

(d) Ray arrival rate fit for scenario II ($1/\lambda = 3.35 \quad ns$)

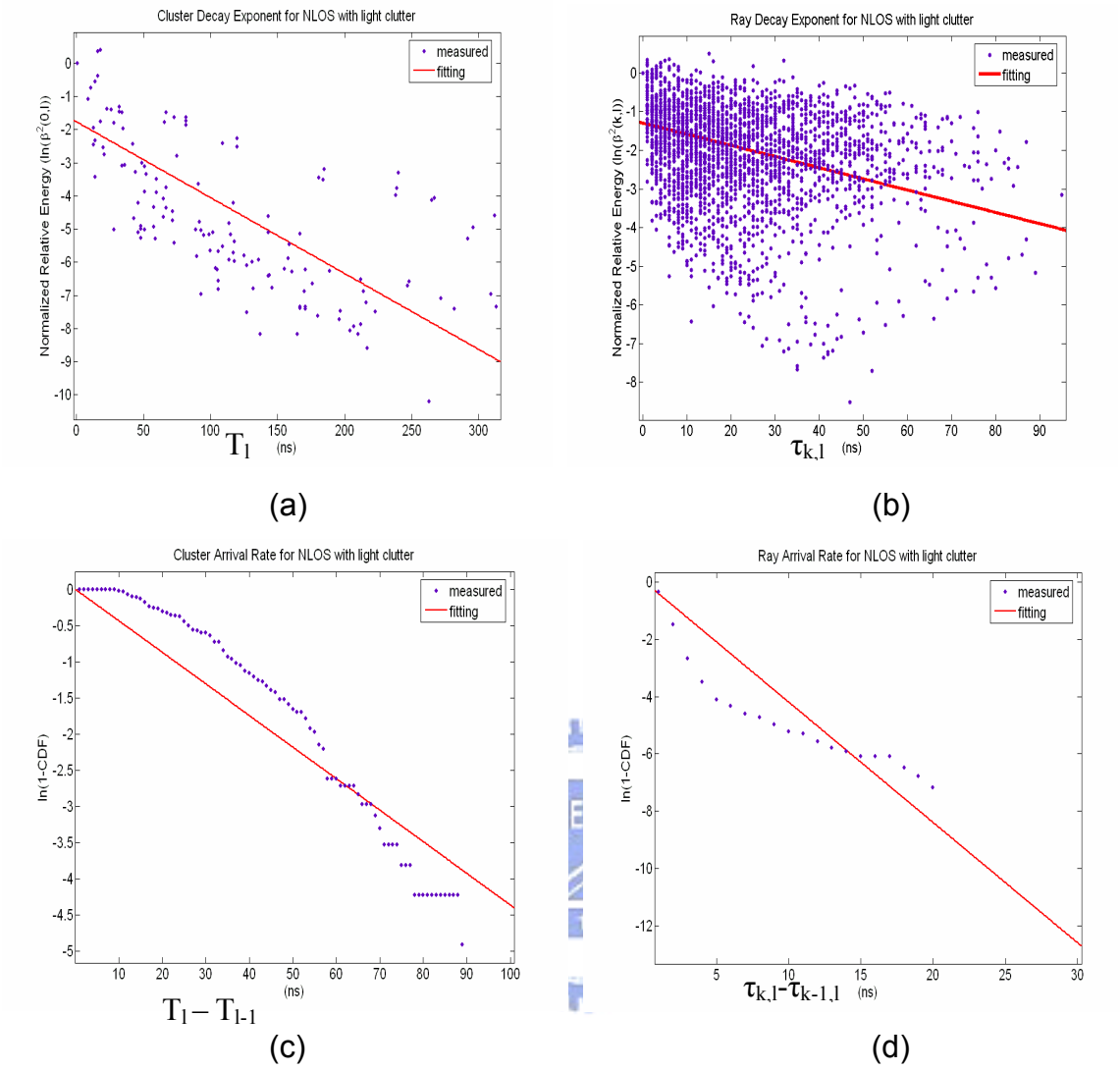

Fig 5-4 Four parameters of S-V model for scenario III

(a) Cluster decay exponent fit for scenario III ($\Gamma = 43.68 \quad ns$)

(b) Ray decay exponent fit for scenario III ($\gamma = 40.37 \quad ns$)

(c) Cluster arrival rate fit for scenario III ($1/\Lambda = 22.91 \quad ns$)

(d) Ray arrival rate fit for scenario III ($1/\lambda = 2.39 \quad ns$)

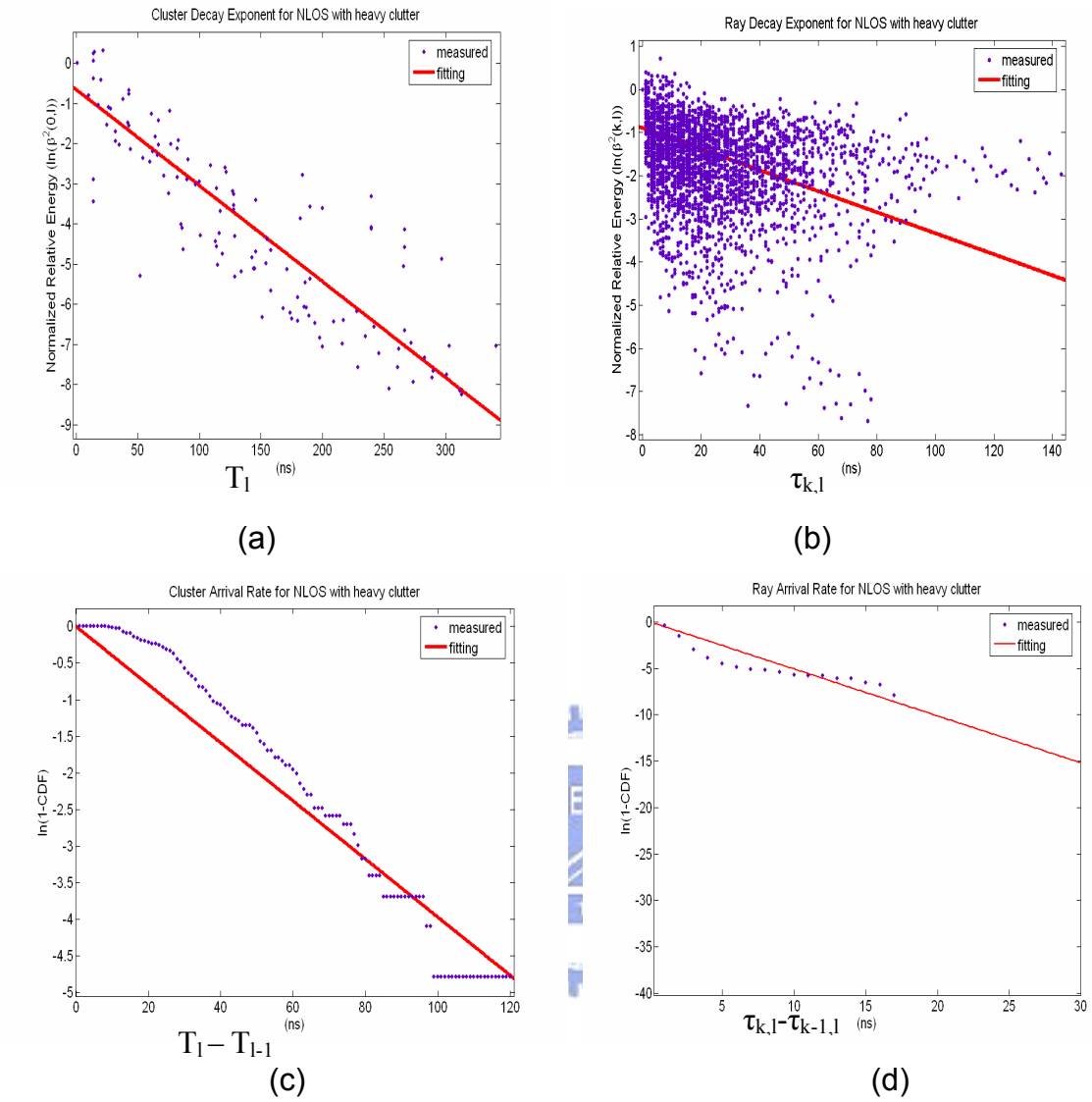

Fig 5-5 Four parameters of S-V model for scenario IV

(a) Cluster decay exponent fit for scenario IV ($\Gamma = 41.84 \quad ns$)

(b) Ray decay exponent fit for scenario IV ($\gamma = 41.1 \quad ns$)

(c) Cluster arrival rate fit for scenario IV ($1/\Lambda = 25.2 \quad ns$)

(d) Ray arrival rate fit for scenario IV ($1/\lambda = 1.98 \quad ns$)

Table 6 Summary of four parameters of S-V model for scenarios I, II, III and IV

	LOS with light clutter	NLOS with light clutter	LOS with heavy clutter	NLOS with heavy clutter
Mean No. of clusters	6.38	7.52	7.17	8.59
Γ	30.47 ns	43.68 ns	27.75 ns	41.84 ns
std	6.06	16.92	4.21	16.37
γ	27.12 ns	40.37 ns	30.77 ns	41.1 ns
std	9.73	21.06	10.66	18.04
$1/\Lambda$	23.7 ns	22.91 ns	20.51 ns	25.2 ns
$1/\lambda$	4.47 ns	2.39 ns	3.35 ns	1.98 ns

5.4 Analysis of Measured results

Table 6 is a summary of four parameters of S-V model for scenarios I, II, III and IV. From Comparing scenasios I and III, we can see that Γ decay faster in the LOS condition than in the NLOS condition. This is because that in the LOS condition, direct path is stronger than others. The same tread is find between scenario II and IV.

From [19] we can see that in the broadbasnd system, Γ、γ have different decay slope, but we find that in the UWB system Γ 、 γ have similar decay slope from our measured results.

Chapter 6

Hybrid UWB MIMO Channel Model

In this chapter, we propose a set of channel models applicable to indoor UWB-MIMO systems. The newly developed UWB MIMO channel models are based on 802.11n channel model [12] to modify and combing UWB channel model.

A step-wise development of the new models follows: In each of the four models (A-D) distinct clusters were identified first. The number of clusters varies from 6 to 9, depending on the model. The power of each tap in a particular cluster was determined by using the parameter of above UWB channel model (chapter 5). Next, angular spread (AS), angle-of-arrival (AOA) and angle of departure (AOD) values were assigned to each tap and cluster (using statistical methods) that agrees with experimentally determined values reported in the literature. Cluster AS was experimentally found to be in the 20^{o} to 40^{o} range [10, 11, 22-25] and the mean AOA was found to be random with a uniform distribution. With the knowledge of each tap power, AS, and AOA (AOD), for a given antenna configuration, the channel matrix H can be determined. The channel matrix H fully describes the propagation channel between all transmit and receive antennas. If the number of receive antennas is n and transmit antennas is m, the channel matrix H has a dimension of n x m. To arrive at channel matrix H, we use a method that employs correlation matrix and i.i.d. matrix (zero-mean unit variance independent complex Gaussian random variables). The correlation matrix for each tap is based on the power

angular spectrum (PAS) with AS being the second moment of PAS [28, 29]. Finally, to verify the newly developed model, we have calculated the channel capacity and compared it to experimentally determined capacity results with good agreement.

6.1 SISO UWB Models

A set of UWB channel models was developed by Chapter 5. Four delay profile models were proposed for different environments (Models A-D):

- Model A: LOS with light clutter.
- Model B: LOS with heavy clutter.
- Model C: NLOS with light clutter.
- Model D: NLOS with heavy clutter.

The path loss model that we use is referenced in [26]. The path loss in dB as a function distance is given by

$$PL(d) = PL_0 + 10 \cdot n \cdot \log_{10}\left(\frac{d}{d_0}\right) + S \qquad d \geq d_0 \tag{6-1}$$

where *PL(d)* represents the received power at a distance *d*, computed relative to a reference distance *do* i.e. *do* = 1m and PL_o is the free-space PL in the far-field of the antennas at a reference distance *do*. PL_o is the interception point and usually is calculated based on the mid-band frequency. *n* is the PL exponent and *S* is the shadowing fading parameter. The parameters of path loss model are summarized in table 7. In the table 7, shadowing fading parameter is given by the term *S* that varies randomly from one location to another location. It is a zero mean Gaussian distributed random variables in dB with standard deviation σs which is also in dB.

Table 7 Parameters of path loss model

Model	n	PL_o [dB]	σs [dB]
A	1.18	50.1	0.93
B	2.48	46.5	1.50
C	2.18	41.3	1.43
D	2.69	47.3	4.69

6.2 UWB-MIMO Matrix Formulation

We follow the MIMO modeling approach presented in [27, 28] that utilizes receive/transmit correlation matrices and combine UWB channel model. The UWB-MIMO channel matrix *H*, at one instance of time, in the A-D delay profile models can be written as

$$[H(t)] = \sum_{l=0}^{L} \sum_{k=0}^{K} \sqrt{P_{k,l}} [X_{k,l}] \delta(t - T_l - \tau_{k,l}) \tag{6-2}$$

where $P_{k,l}$ is the power of (k,l)-th tap, T_l represents the arrival time of the *l*th cluster, $\tau_{k,l}$ is the arrival time of the *k*th arrival within the *l*th cluster, relative to T_l , $X_{k,l}$ is correlated zero-mean, unit variance, complex Gaussian random variables of (k,l)-th tap and symbol [ ] denote the matrix.

To correlate the matrix $X_{k,l}$, the following method can be used

$$[X_{k,l}] = [R_{rx}^{k,l}]^{1/2} [H_{iid}] ([R_{tx}^{k,l}]^{1/2})^T \tag{6-3}$$

where $R_{tx}^{k,l}$ and $R_{rx}^{k,l}$ are the receive and transmit correlation matrix of (k,l)-th tap, respectively, and H_{iid} is a matrix of independent zero mean, unit variance, complex Gaussian random variables.

Transmit and receive correlation matrix for each (k,l)-th tap are

$$R_{tx}^{k,l} = \begin{bmatrix} 1 & \rho_{tx12}^{k,l} & \cdots & \rho_{tx1M}^{k,l} \\ \rho_{tx21}^{k,l} & 1 & \cdots & \rho_{tx2M}^{k,l} \\ \vdots & \vdots & \ddots & \vdots \\ \rho_{txM1}^{k,l} & \rho_{txM2}^{k,l} & \cdots & 1 \end{bmatrix}$$

$$R_{rx}^{k,l} = \begin{bmatrix} 1 & \rho_{rx12}^{k,l} & \cdots & \rho_{rx1N}^{k,l} \\ \rho_{rx21}^{k,l} & 1 & \cdots & \rho_{rx2N}^{k,l} \\ \vdots & \vdots & \ddots & \vdots \\ \rho_{rxN1}^{k,l} & \rho_{rxN2}^{k,l} & \cdots & 1 \end{bmatrix} \quad (6\text{-}4)$$

The complex correlation coefficient values calculation for each tap is based on the power angular spectrum (PAS) with angular spread (AS) being the second moment of PAS [28, 29]. Using the PAS shape, AS, mean angle-of-arrival (AOA), and individual tap powers, correlation matrices of each tap can be determined as described in [28]. For the uniform linear array (ULA) the complex correlation coefficient at the linear antenna array is expressed as

$$\rho^{k,l} = R_{XX}^{k,l}(D) + jR_{XY}^{k,l}(D) \quad (6\text{-}5)$$

where $D = 2\pi d / \lambda$, and $R_{XX}^{k,l}$ and $R_{XY}^{k,l}$ are the cross-correlation functions between the real parts (equal to the cross-correlation function between the imaginary parts) and between the real part and imaginary part for each (k,l)-th tap, respectively, with

$$R_{XX}^{k,l}(D) = \int_{-\pi}^{\pi} \cos(D\sin\phi) PAS^{k,l}(\phi) d\phi \quad (6\text{-}6)$$

and

$$R_{XY}^{k,l}(D) = \int_{-\pi}^{\pi} \sin(D\sin\phi) PAS^{k,l}(\phi) d\phi \quad (6\text{-}7)$$

Next we briefly describe the various steps in our cluster modeling approach. We

- Start with delay profiles of models A-D.
- Manually identify clusters in each of the four models.
- Assume PAS shape of each cluster and corresponding taps (Laplacian).
- Assign AS to each cluster and corresponding taps.
- Assign mean AOA (AOD) to each cluster and corresponding taps.
- Assume antenna configuration.
- Calculate correlation matrices for each tap.

In the next section we elaborate on the above steps.

6.3 Cluster Modeling Approach

6.3.1 PDP Shape

For our modeling purposes we uses the results of Chapter 5. We put our parameter of S-V model into 802.15.3a channel model so as to determine the model A-D delay profiles.

6.3.2 PAS Shape

The angle of arrival statistics within a cluster were found to closely match the Laplacian distribution [10, 11, 25]

$$p(\theta) = \frac{1}{\sqrt{2}\sigma} e^{-\left|\sqrt{2}\theta/\sigma\right|} \tag{6-8}$$

where σ is the standard deviation of the PAS (which corresponds to the numerical value of AS).

6.3.3 Mean AOA (AOD) of Each Cluster

It was found in [10, 11] that the relative cluster mean AOAs have a random uniform distribution over all angles.

In our model, we assume that the relative cluster mean AODs also have a random

uniform distribution over all angles. We assume this since for indoor WLANs, the multipath reflectors tend to be similar for both the access point (AP) and the client (STA).

Use Model A as an example, where there are 6 clusters. The 6 mean AOAs were set by randomly generating 6 values from a uniform distribution over [0, 2π]. Similarly, the 6 mean cluster AODs were set by randomly generating 6 different values from the uniform distribution over [0, 2π], uncorrelated from the six AOA values.

The AOAs and AODs for other models were similarly computed.

6..3.4 AS of Each Cluster

In [10] the mean cluster AS values were found to be 21^o and 25^o for two buildings measured. In [11] the mean AS value was found to be 37^o. To be consistent with these findings, we select the mean cluster AS values for models A-D in the 20^o to 40^o range. To assign an AS value to each cluster within a particular model, we use observations from outdoor channels. For outdoor environments, it was found that the cluster rms delay spread (DS) is highly correlated (0.7 correlation coefficient) with the AS [30]. It was also found that the cluster rms delay spread and AS can be modeled as correlated log-normal random variables. We apply this intuitive finding to models A-D using the following procedure (we note that the DS are calculated from the experimental data and AS values are determined following the procedure described below)

- Calculate rms DS of each cluster, convert to dB values ($10\log_{10}n$, where n is rms delay spread in nanoseconds).
- For each model, calculate the mean rms DS and corresponding standard deviation, σ_d (dB).
- Determine the mean cluster AS in dB ($10\log_{10}m$, where m is AS in degrees) proportionally (linear dependence) to the mean cluster rms DS values using the following formula (the resulting mean AS is in the 20^o to 40^o range)

$$\overline{AS} = 0.32\overline{DS} + 9.88 \quad \text{(dB)} \qquad \text{(6-9)}$$

The model-dependent cluster DS and AS can be represented in the following form

$$DS = \overline{DS} + \sigma_d x \qquad \text{(dB)} \qquad \text{(6-10)}$$

$$AS = \overline{AS} + \sigma_a y \qquad \text{(dB)} \qquad \text{(6-12)}$$

where x and y are zero-mean, unit-variance Gaussian random variables and σ_d and σ_a are standard deviations, respectively.

- We further assume that $\sigma_a = \sigma_d$, and that the correlation coefficient between the Gaussian random variables x and y is 0.7.
- Using the following formula we can determine y, with x known

$$y = \rho x + \sqrt{1-\rho^2}\, z \qquad \text{(6-12)}$$

where ρ is the correlation coefficient and z is an independent zero-mean unit-variance Gaussian random variable.

The above procedure results in a lower AS for models with lower rms delay spread and larger AS for models with larger rms delay spread. For the transmit side, an independent set of AS was generated similar to the results in the receive side (cluster AS at receiver does not have to necessarily match the cluster AS at the transmitter).

Table 8 Mean and Standard Deviation of Cluster RMS Delay Spreads for each model

Model	Mean Cluster DS (dB)	Std. Dev. Cluster DS (dB)
A	10.51	1.3
B	13.61	2.01
C	11.3125	2.5
D	14.786	1.7

Note that the mean DS for the transmitter is assumed to be equal to the mean DS for the receiver. Also, the mean AS for the transmitter is assumed to be equal to the mean

AS for the receiver. In other words, the values inserted into (6-9) are identical for both transmit and receive. However, different random values for DS and AS are used for the transmitter versus the receiver. Equations (6-10) and (6-11) are executed once for the transmitter. Equations (6-10) and (6-11) are then executed again for the receiver.

6.3.5 Doppler Spectrum

The fading characteristics of the indoor wireless channels are very different from the one we know from the mobile case. In indoor wireless systems transmitter and receiver are stationary and people are moving in between, while in outdoor mobile systems the user terminal is often moving through an environment. As a result, a function $S(f)$ has to be defined for indoor environments in order to fit the Doppler power spectrum measurements [12]. $S(f)$ can be expressed as (in linear values, not dB values):

$$S(f) = \frac{1}{1 + A\left(\frac{f}{f_d}\right)^2} \tag{6-13}$$

where A is a constant, used to define the $0.1\,S(f)$, at a given frequency f_d, being the Doppler Spread.

$$\left(S(f)\right)\Big|_{f=f_d} = 0.1, \text{ so, } A = 9 \tag{6-14}$$

The Doppler spread f_d is defined as

$$f_d = \frac{v_o}{\lambda} \tag{6-15}$$

where v_o is the environmental speed determined from measurements that satisfy (6-14), and λ is the wavelength defined by

$$\lambda = \frac{c}{f_c} \tag{6-16}$$

where c is the light speed and f_c is the carrier frequency. The value for v_o is proposed equal to 1.2 km/h [12].

6.4 Simulated UWB-MIMO Channel Properties Using Matlab Program

In this section we determine some of the important properties of the simulated channel matrices *H*, specifically channel capacity. For the simulation, we use the following antenna configuration system

- 4 transmit and 4 receive antennas (4x4 UWB-MIMO system)
- Uniform linear array (ULA)
- $\lambda/2$ adjacent antenna spacing
- Isotropic antennas
- No antenna coupling effect
- All antennas with same polarization (vertical)

Figure 6-1、6-2、6-3、6-4 shows cumulative distribution functions (CDFs) of capacity for Models A-D including measured data, 802.11n channel model and i.i.d. case (channel matrix elements are i.i.d., zero-mean unit-variance complex Gaussian random variables) assuming ρ= 10 dB, 2000 channel realizations, and 4x4 UWB-MIMO system.

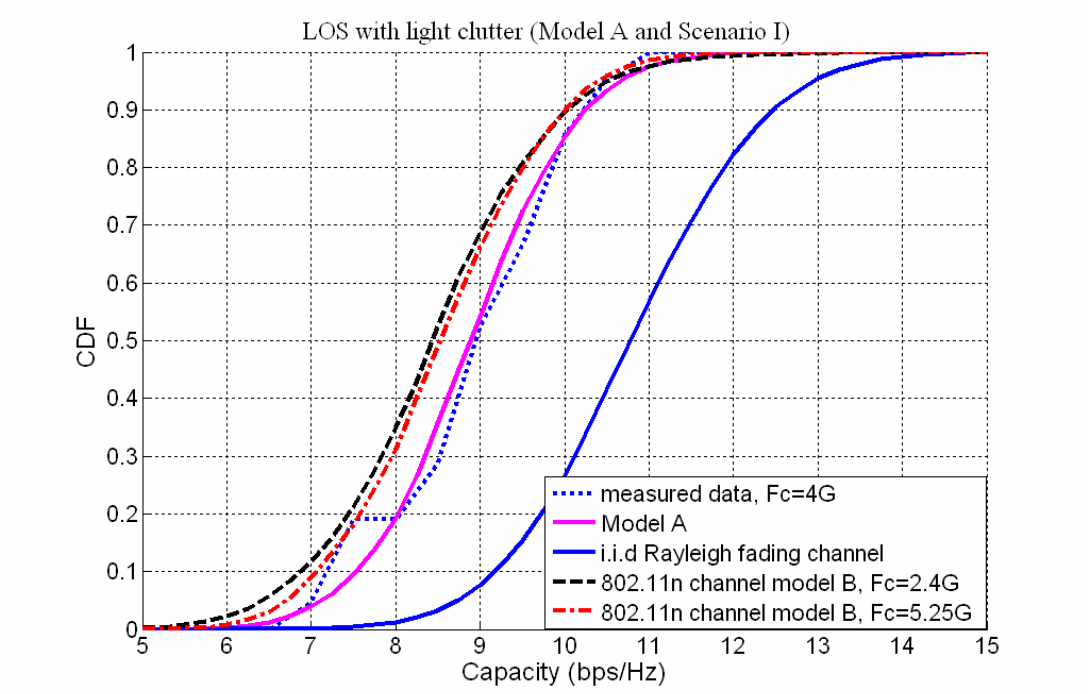

Fig.6-1 Computed and measured 4×4 UWB-MIMO capacity CDF for model A and scenario I.

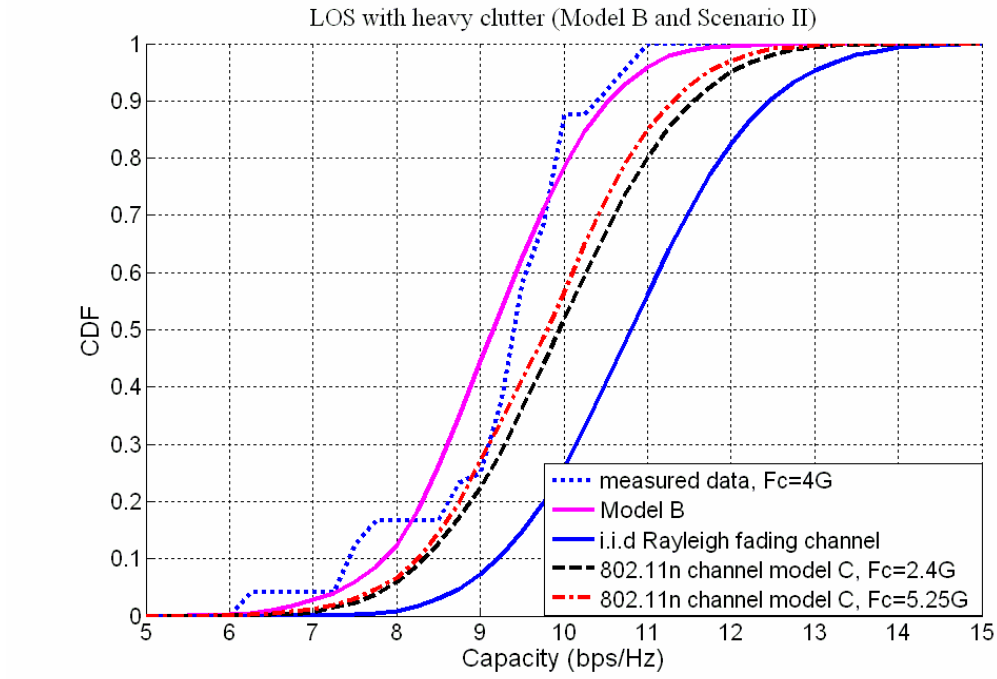

Fig.6-2 Computed and measured 4×4 UWB-MIMO capacity CDF for model B and scenario II.

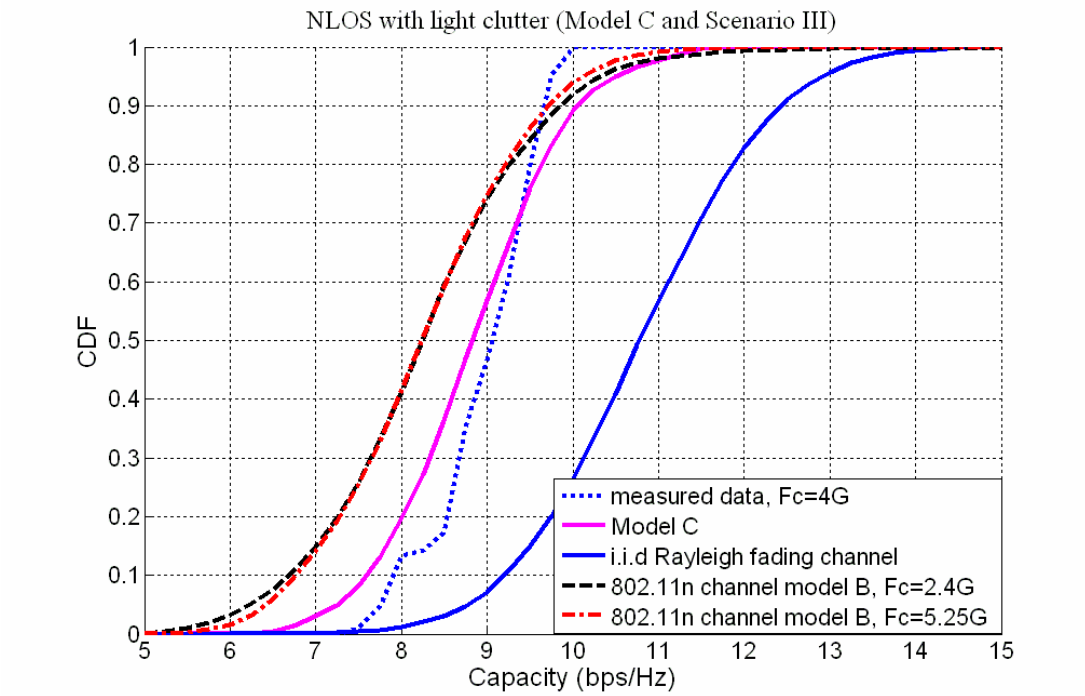

Fig.6-3 Computed and measured 4×4 UWB-MIMO capacity CDF for model C and scenario III.

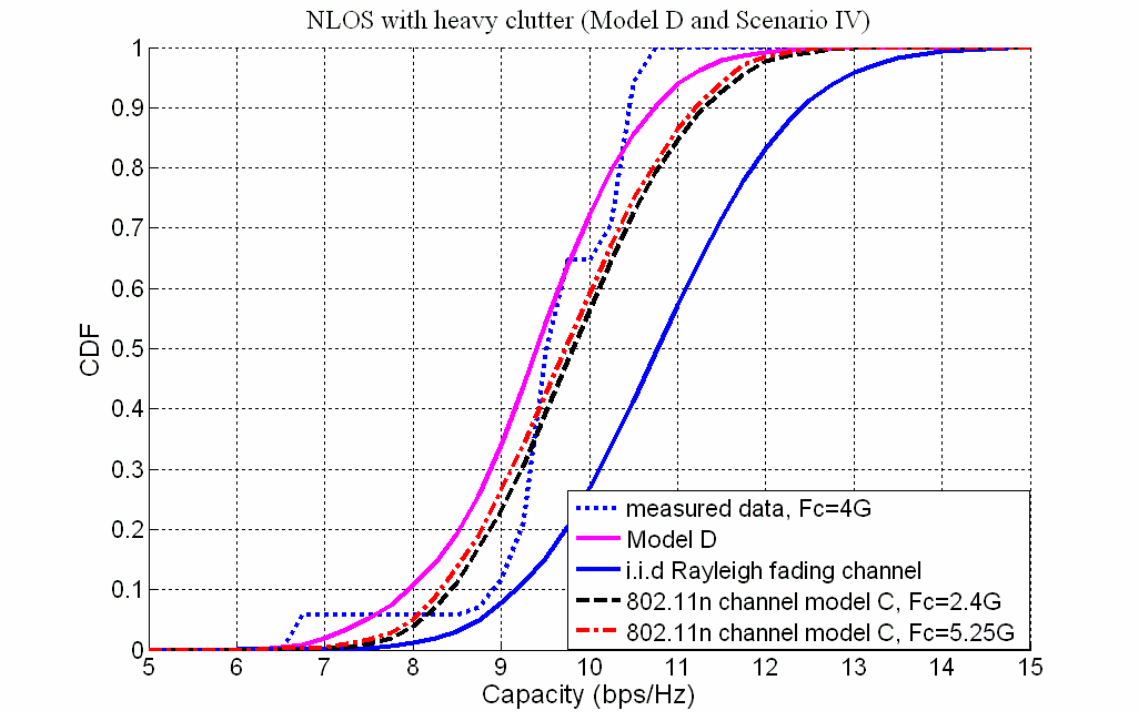

Fig.6-4 Computed and measured 4×4 UWB-MIMO capacity CDF for model D and scenario IV.

Table 9 Capacity of our simulated model, 802.11n channel model and measured results

	Mean of capacity and std (bps/Hz)			
	for measurement	**for UWB-MIMO model**	**for 802.11n model (2.4G)**	**for 802.11n model (5.25G)**
Scenario I	**9.1583** 1.0523	**9.0165** 1.0602	**8.5768** 1.2426	**8.665** 1.118
Scenario II	**9.2861** 1.0592	**9.2872** 1.0658	**10.0703** 1.2438	**9.8885** 1.1967
Scenario III	**9.0798** 0.6103	**8.9661** 0.978	**8.3814** 1.1954	**8.363** 1.0987
Scenario IV	**9.6954** 0.903	**9.5052** 1.0787	**9.9659** 1.0913	**9.8623** 1.1001

Table 9 shows mean capacity and STD of our UWB-MIMO channel model, 802.11n channel model and measured results for each model.

From table 9 we can see that our computed results match very well with measured results. For the models B and D it is expected that capacity is higher because of the more clusters present with wider AS when compared to the models A and C.

Chapter 7

Conclusion

In this thesis, capacity, EDOF and correlations have been measured to analyze the effects of propagation, array arrangement and bandwidth on a 4x4 UWB-MIMO system. The array arrangement includes antenna array spacing and array orientation. Six propagation scenarios are included to give a complete study of the effects. The measurement using Agilent 8719ET vector network analyzer was carried out in the National Chiao Tung University campus.

We develop indoor UWB-MIMO channel model. We first present the characterization of UWB channels for indoor environment with our measurements. Then we base on 802.11n channel model to modify and combing UWB channel model to develop UWB-MIMO channel model. Finally, we verify our channel model with our measured data.

In this research, some phenomena are observed and listed as following:

(1) Propagation distance effect: The UWB-MIMO capacity is dependent of Tx-Rx distance in LOS with light clutter, i.e. capacity is lower when Tx-Rx distance in small AS (Angular Spread) of AOA/AOD. And capacity is independent of Tx-Rx distance in the environment with heavy clutter, i.e. capacity is similar for any Tx-Rx distance when AS of AOA/AOD is large. It is reported in the literature [16] that in a “wave guiding” environment the capacity decreases as the Tx-Rx distance increases. In this thesis, we choose four paths in the lobby and laboratory representing LOS/NLOS with light/heavy clutter (scenarios I/II/III/IV) but different from the environment in [16]. Our result is

different from [16]. This is because long distance in the hall the dominant signal component will be the LOS component and the angular spread is limited, thus substantially increases the correlations and results in lower capacity in the literature [16] but not the condition in our measurement sites.

(2) Local scatterers effect: local scatterers around tx/rx array will affect the capacity, i.e. enhance UWB-MIMO performance. This is because the local scatterers reflect more multipath and more multipath result in low correlation coefficient and then obtain higher capacity.

(3) Antenna spacing effect: measurement results in this thesis show that antenna spacing may affect UWB-MIMO capacity and correlations under any environment (scenarios I/II/III/IV). Furthermore the UWB-MIMO capacity increases as the antenna spacing increases and it saturates when the spacing is larger than 0.5λ. This reveals that the correlation distance between the elements in indoor environments is about 0.5λ.

(4) Antenna array orientation effect: in a 'wave guiding' environment such as a long corridor (scenarios V/VI), a significant difference in capacity is observed when the linear receiver array orientation is changed from parallel to perpendicular (to the LOS). In a 'non wave guiding' environment such as laboratory (scenarios II/IV), there is no remarkable discrepancy between results of different orientations.

(5) Capacity Loss: for a more in-depth analysis of the performance of UWB-MIMO systems, measurements were done to investigate the effects of SNR and antenna correlation on UWB-MIMO channel capacity. For small antenna spacing, when SNR increases, the channel capacity loss increases initially but decreases gradually afterwards. It means that in small antenna spacing, the relative channel capacity loss due to the effect of high antenna correlation is reduced as SNR increases. In other words the UWB-MIMO system is robust against the high antenna correlation when SNR is high.

When Tx-Rx distance is in near distance, although antenna correlation is high but if received SNR is excess 10dB then the UWB-MIMO system is robust against the antenna correlation. From above results, we find that the loss of channel capacity owing to high correlation is significantly reduced when the SNR is sufficiently high.

(6) Bandwidth effect: our results show a small difference in capacity when using the larger bandwidth. Hence not much frequency diversity is available.

(7) UWB channel model: from the parameter of S-V model in UWB radio channel model, we can see that Γ decay faster in the LOS condition than in the NLOS condition. From [19] we can see that in the broadband system, Γ 、γ have different decay slope, but we find that in the UWB system Γ 、γ have similar decay slope from our measured results.

(8) UWB MIMO channel model: the UWB-MIMO channel model has been proved to be effective and accurate.

Reference

[1] G. J. Foschini, "*Layered space-time architecture for wireless communication in a fading environment when using multi-element antennas*,"AT&T Bell Labs. Tech. J., pp. 41–59, 1996.

[2] D-S Shiu, G.J. Foschini, M.J. Gans, and J.M. Kahn. "*Fading Correlation and Its Effect on the Capacity of Multielement Antenna systems*". IEEE Trans. on Communications, 48(3):502–513, March 2000.

[3] Pohl, V.; Jungnickel, V.; Haustein, T.; von Helmolt, C. "*Antenna Spacing in MIMO Indoor channels*," Vehicular Technology Conference, 2002. VTC Spring 2002, IEEE 55th , Volume: 2 , 6-9 May 2002 ,Page(s): 749 -753 vol.2

[4] Elnaggar, M.; Safavi-Naeini, S.; Chaudhuri, S.K. "*Effect of oversimplifying the simulated indoor propagation on the deterministic mimo capacity*" Electrical and Computer Engineering, 2004. Canadian Conference on Volume 1, 2-5 May 2004 Page(s):221 - 224 Vol.1

[5] Svantesson, T.; Wallace, J.; "*On signal strength and multipath richness in multi-input multi-output systems*" Svantesson, T.; Wallace, J.;Communications, 2003. ICC '03. IEEE International Conference on Volume 4, 11-15 May 2003 Page(s):2683 - 2687 vol.4

[6] Jeng-Shiann Jiang; Ingram, M.A.,"*Enhancing measured MIMO capacity by adapting the locations of the antenna elements",* Personal, Indoor and Mobile Radio Communications, 2002. The 13th IEEE International Symposium on, vol.3, pp.1027 – 1031, Sept. 2002

[7] Ozcelik, H.; Herdin, M.; Hofstetter, H.; Bonek, E.; "*Capacity of different MIMO systems based on indoor measurement at 5.2G*" Personal Mobile Communications Conference,2003. 5th European (Conf. Publ. No. 492)22-25 April 2003 Page(s):463 - 466

[8] Almers, P.; Tufvesson, F.; Karlsson, P.; Molisch, A.F.; "*The effect of horizontal array orientation on MIMO channel capacity*" Vehicular Technology Conference, 2003. VTC 2003-Spring. The 57th IEEE Semiannual Volume 1, 22-25 April 2003 Page(s):34 - 38 vol.1

[9] Kim, C.W.; Sun, X.; Chiam, L.C.; Kannan, B.; Chin, F.P.S.; Garg, H.K.; "*Characterization of Ultra-wideband for outdoor office environment*" Wireless Communications and Networking Conference, 2005 IEEE Volume 2, 13-17 March 2005 Page(s):950 - 955 Vol. 2

[10] Q.H. Spencer, et al., "*Modeling the statistical time and angle of arrival characteristics of an indoor environment*," *IEEE J. Select. Areas Commun.*, vol. 18, no. 3, March 2000, pp. 347-360.

[11] R.J-M. Cramer, R.A. Scholtz, and M.Z. Win, "*Evaluation of an ultra-wide-band propagation channel*," *IEEE Trans. Antennas Propagat.*, vol. 50, no.5, May 2002, pp. 561-570.

[12] "*IEEE P802.11 TGn Channel Models*", described in document IEEE 802.11-03/940r4, May 2004.

[13] Lin Zhiwei; Premkumar, B.; Madhukumar, A.S. "*MMSE detection for high data rate UWB MIMO systems*"; Vehicular Technology Conference, 2004. VTC2004-Fall. 2004 IEEE 60th Volume 2, 26-29 Sept. 2004 Page(s):1463 - 1467 Vol. 2

[14] Siriwongpairat, W.; Olfat, M.; Liu, K.J.R.; "*On the performance evaluation of TH and DS UWB MIMO systems*" Wireless Communications and Networking Conference, 2004. WCNC. 2004 IEEEVolume 3, 21-25 March 2004 Page(s):1800 - 1805 Vol.3

[15] J. P. Kermoal, P. E. Mogensen, S.H. Jensen, J.B. Andersen, F. Frederiksen, T.B. Sorensen and K. I. Pedersen, *"Experimental Investigation of Multipath Richness for Multi-Element Transmit and Receive Antenna Arrays,"* IEEE Proc. Vehicular Technology Conference, pp. 2004-2008, Tokyo, Japan, May 2000

[16] R. G. Gallager, *"Information Theory and Reliable Communication,"* Wiley, 1968.

[17] D. P. Palomar, J. R. Fonollosa, and M. A. Lagunas, *"Capacity results of spatially correlated frequency-selective MIMO channels in UMTS,"* in Proc. IEEE VTC'01, vol. 2, 2001, pp. 553–557.

[18] Elnaggar, M.; Safavi-Naeini, S.; Chaudhuri, S.K., "*Effect of oversimplifying the simulated indoor propagation on the deterministic MIMO capacity*," Electrical and Computer Engineering, 2004. Canadian Conference on Volume 1, 2-5 May 2004 Page(s):221 - 224 Vol.1

[19] A.A. Saleh, R.A. Valenzuela, "*A statistical model for indoor multipath propagation*," *IEEE J. Sel. Areas Commun,* Vol. 5, No. 2, pp. 128-137, Feb. 1987.

[20] Pal, A.; Chor Min Tan; Beach, M.A, *"Comparision of MIMO channels from multipath parameter extraction and direct channel measurements,"* Personal, Indoor and Mobile Radio Communications, 2004. PIMRC 2004. 15th IEEE International Symposium on Volume 3, 5-8 Sept. 2004 Page(s):1574 – 1578

[21] Kyritsi, P.; Cox, D.C, *"Correlation Properties of MIMO Radio Channels for Indoor Scenarios,"* Signals, Systems and Computers, 2001 Conference Record of the Thirty-Fifth Asilomar Conference on, Volume: 2, 4-7 Nov. 2001, pp. 994 -998 vol.2

[22] A.S.Y. Poon and M. Ho, "*Indoor multiple-antenna channel characterization from 2 to 8 GHz*," *submitted to ICC 2003 Conference*.

[23] G. German, Q. Spencer, L. Swindlehurst, and R. Valenzuela, "*Wireless indoor channel modeling: Statistical agreement of ray tracing simulations and channel sounding measurements*," *in proc. IEEE Acoustics, Speech, and Signal Proc. Conf.*, vol. 4, 2001, pp. 2501-2504.

[24] J-G. Wang, A.S. Mohan, and T.A. Aubrey, "*Angles-of-arrival of multipath signals in indoor environments,*" *in proc. IEEE Veh. Technol. Conf.*, 1996, pp. 155-159.

[25] Chia-Chin Chong, David I. Laurenson and Stephen McLaughlin, "*Statistical Characterization of the 5.2 GHz wideband directional indoor propagation channels with clustering and correlation properties*" *in proc. IEEE Veh. Technol. Conf.*, vol. 1, Sept. 2002, pp. 629-633.

[26] Chia-Chin Chong; Youngeil Kim; Seong-Soo Lee; "*Statistical characterization of the UWB propagation channel in various types of high-rise apartments*" Wireless Communications and Networking Conference, 2005 IEEE Volume 2, 13-17 March 2005 Page(s):944 - 949 Vol. 2

[27] J.P. Kermoal, L. Schumacher, P.E. Mogensen and K.I. Pedersen, "*Experimental investigation of correlation properties of MIMO radio channels for indoor picocell scenario,*" *in Proc. IEEE Veh. Technol. Conf.*, Boston, USA, vol. 1, Sept. 2000, pp. 14-21.

[28] L. Schumacher, K. I. Pedersen, and P.E. Mogensen, "*From antenna spacings to theoretical capacities – guidelines for simulating MIMO systems,*" in *Proc. PIMRC Conf.*, vol. 2, Sept. 2002, pp. 587-592.

[29] J. Salz and J.H. Winters, "*Effect of fading correlation on adaptive arrays in digital mobile radio,*" *IEEE Trans. Veh. Technol.*, vol. 43, Nov. 1994, pp. 1049-1057.

[30] K.I. Pedersen, P.E. Mogensen, and B.H. Fleury, "*A stochastic model of the temporal and azimuthal dispersion seen at the base station in outdoor propagation environments,*" *IEEE Trans. Veh. Technol.*, vol. 49, no. 2, March 2000, pp. 437-447.

[31] L. H. Brandenburg and A. D.Wyner, *"Capacity of the Gaussian channel with memory: The multivariate case,"* Bell Syst. Tech. J., vol. 53, no. 5, pp. 745–778, 1974.

[32] Jorgen Bach Andersen, "*Array Gain and Capacity for Known Random Channels with Multiple Element Arrays at Both Ends,"* IEEE Journal on Selected Areas in Communications, vol. 18, no. 11, pp. 2171-2178, November 2000

[33] G.G. Rayleigh and J.M. Cioffi. "*Spatio-Temporal Coding for Wireless Communication"*. IEEE Trans. on Communications, 46(3):357–366, March 1998

[34] D. Chizhik, G. J. Foschini, and R. A. Venezuela, *"Capacities of multi-element transmit and receive antennas: Correlation and keyholes,*" Electron. Lett., vol. 36, pp. 1099–1100, June 2000.